Canadian Science Publishing | Arctic Science

Long-term ice-rich permafrost coast sensitivity to air temperatures and storm influence: lessons from Pullen Island, N.W.T.

Journal:	*Arctic Science*
Manuscript ID	AS-2020-0003.R1
Manuscript Type:	Article
Date Submitted by the Author:	20-May-2020
Complete List of Authors:	Berry, H. Bay; Geological Survey of Canada Atlantic, ; Dalhousie University, Earth and Environmental Sciences Whalen, Dustin; Geological Survey of Canada Atlantic Lim, Michael; Northumbria University, Engineering and Environment
Keyword:	coastal erosion, permafrost, slope instability, arctic climate change
Is the invited manuscript for consideration in a Special Issue? :	Not applicable (regular submission)

Long-term ice-rich permafrost coast sensitivity to air temperatures and storm influence: lessons from Pullen Island, N.W.T.

H. Bay Berry [a b], Dustin Whalen [a], Michael Lim [c]

[a] Geological Survey of Canada, Bedford Institute of Oceanography, 1 Challenger Drive, Dartmouth, Nova Scotia B2Y 4A2, Canada

[b] Dalhousie University, Department of Earth Sciences, 1459 Oxford Street, Halifax, Nova Scotia B3H 4R2, Canada

[c] Northumbria University, Engineering and Environment, Ellsion Building, Northumberland Road, Newcastle upon Tyne NE1 8ST, UK

Abstract

Response of erosive mechanisms to climate change is of mounting concern on Beaufort Sea coasts, which experience some of the highest erosion rates in the Arctic. Collapse of intact permafrost blocks and slumping within sprawling retrogressive thaw complexes are two predominant mechanisms that manifest as cliff retreat in this region. Using aerial imagery and ground survey data from Pullen Island, N.W.T., Canada, from 13 time points between 1947 and 2018, we observe increasing mean retreat rates from 0 ± 4.8 m/a in 1947 to 12 ± 0.3 m/a in 2018. Mean summer air temperature was positively correlated with cliff retreat over each time step via block failure ($r^2 = 0.08$; $p = 0.5$) and slumping ($r^2 = 0.41$; $p = 0.05$), as was mean storm duration with cliff retreat via block failure ($r^2 = 0.84$; $p = 0.0002$) and slumping ($r^2 = 0.34$; $p = 0.08$). These data indicate that air temperature has a greater impact in slump-dominated areas, while storm duration has greater control in areas of block failure. Increasingly heterogeneous cliff retreat rates are likely resulting from different magnitudes of response to climate trends depending on mechanism, and on geomorphological variations that prescribe occurrences of retrogressive thaw slumps.

Key words: coastal erosion, permafrost, slope instability, arctic climate change.

1. Introduction

The ice-rich nature of the Beaufort Sea permafrost coasts has contributed to widespread, rapid coastal retreat. Even with the processes which drive erosion in this setting being restricted to the few open-water months each year (Aré, et al., 2008), the reported mean coastal retreat rate for most areas of the Canadian Beaufort Sea in the late 20th and early 21st century was 1 m a^{-1}, with some locations experiencing upwards of 20 m of retreat in a single season (Table 1; Harper, 1990; Solomon, 2005; Radosavljevic, et al., 2016).

Ground ice in permafrost soils may be present in as pore ice, take the form of lenses, veins, and blocks, or comprise its own stratigraphic unit below the upper layer of sediment (Mackay, 1972; Murton, et al., 2004). While meltwater provides a medium of downlope transport for eroded soil constituents, the high ice-content of the ground material also means that only a fraction of the volume of eroded material contributes to the nearshore sediment budget (Kokelj, et al., 2009b; Dalimore, et al., 1996). Indeed, the Mackenzie River has been estimated to contribute approximately ten times more sediment annually to the Canadian Beaufort Sea than coastal erosion (Rachold, et al., 2000). The rate and variability of coastal erosion in the Canadian Beaufort Sea is affected by intrinsic factors, including ground material, ground-ice and permafrost occurrence, and coastal geomorphology, and by extrinsic variables, such as storm intensity and sea ice occurrence as controlled by atmospheric and hydrodynamic forcing (Solomon, 2005; Manson & Solomon 2007).

Increased retrogressive thaw slump (RTS; or “retrogressive thaw failure”; Couture, et al., 2015) activity since the 1950s has been observed on the western Beaufort Sea coast; these features are characterized by rapid local headwall retrogression due to exposed ground ice melt, creating bowl-shaped structures with steep headwalls of exposed ice-rich permafrost and thawed sediments in the slump floor (Ramage, et al., 2017; Lantuit & Pollard, 2008; Burn & Lewkowicz, 1990). The RTS morphology is in contrast to slumping coastal cliffs (Lantuit & Pollard 2005); although the thaw-related mobilization of ground material is similar in both instances, retreat in an RTS occurs rapidly from a point where ground ice is exposed, wheareas the coastal cliffs erode across long stretches at a relatively uniform rate, resulting in straighter cliff lines (Fig. 1).

Coastal retreat has implications from a terrain-loss perspective and for its potential chemical and atmospheric impact. The regression of coastlines, resulting in highly disturbed terrain or mobilization of ground material to the neashore, impinges on sensitive regions such as terrestrial ecosystems (Environment Canada, 2014), infrastructure and cultural sites of coastal communities (Mackay, 1986), and industrial infrastructure and waste storage sites (Kokelj & GeoNorth Ltd, 2002). Knowledge of erosive processes, trends and future threats is integral to predicting the future viability of the region as a subsistence-use region, and for any potential infrastructure or hydrocarbon development.

In addition to physical threat to terrestrial systems and land-use, coastal retreat of permafrost cliffs also act as a store of organic carbon, which may be liberated to the marine environment and to the atmosphere (Hugelius, et al., 2014). Organic carbon stored in the upper layers of sediment that is remobilized during erosion of ground material may be accumulated on the slope or shore, be incorporated into the nearshore sediment budget along with nitrogen and nutrient soil components, or can be released to the atmosphere by microbial mineralization (Cassidy, et al., 2016; Tanski, et al., 2017). While the amount of carbon dioxide released to the atmosphere is small in magnitude, it may be enough to offset the carbon sequestration of undisturbed tundra in the same region, resulting in a net positive contribution over the course of a growing season (Cassidy, et al., 2016).

Pullen Island, on the outer Mackenzie Delta, Northwest Territories (Fig. 2) has been observed intermittently for over seven decades, via aerial photography and ground surveys. The island’s western cliffs are eroding via slumping and block failure, (Couture, et al., 2015), which is occuring over a relatively small area that is uniformly subject to extinsic environmental conditions. These long-term observations and the ability to differentiate erosion mechanisms affords an opportunity to assess specific geomorphic responses under recent changes in mean annual temperatures and storm intensities. We analyzed erosion processes resulting in cliff retreat, and sensitivities to summer air temperatures and storm events in order to investigate future trends under warming Arctic temperatures. Aerial imagery and ground survey data from 1947 to 2018 were used to determine cliff position and the dominant mechanism resulting in cliff retreat. Weather data from the Environment and Climate Change Canada station at Tuktoyaktuk were available from 1958 to 2018. Due to differences in measurement frequency, the study period used for regressions of weather and cliff retreat was 1967 to 2018.

The definition of "coastline" for this type of study is variable in the literature—broadly speaking, this can be any visually discernable line that separates the terrestrial and marine environments (Boak & Turner, 2005), and examples include the wet-dry line (e.g., Solomon, 2005), the slope base (e.g., Harper, 1978), the cliff edge (e.g., Solomon, et al., 1994), or the vegetation line (e.g. Cunliffe, et al., 2019). As such, in addition to cliff line retreat, this study also addresses two other possible measures of coastal change; shoreline and volumetric change. While in some areas the use of these different lines may yield similar measurements (such as very steep cliffs where the cliff edge and base of slope are inseparable in aerial imagery), these variable measures may have different implications depending on the slope morphology or the focus of the analysis (e.g., terrain loss versus sediment transfer, or marine impacts versus land use). To assess the differences in potential analytical results, "shoreline" retreat was assessed at the base of the slope in addition to the cliff retreat measurement (Fig. 1), as well as the change in volume of material based on Digital Surface Models (DSMs) generated by photogrammetry of imagery from 1992, 2016, 2017, and 2018.

2. Methods

2.1. Study area

Pullen Island, N.W.T., is part of the Mackenzie Delta on the Beaufort Sea shelf (Fig. 2). The island is comprised of tundra uplands and dynamic sand spits. The focus of this study is the west-facing ice-rich cliff; the eroding area includes near-vertical tundra cliffs failing through block collapse, slumping coastal cliffs, and RTS (Couture, et al., 2015). There are no in-depth reports on the state of cliff retreat on Pullen

Island, although it has been included in a multi-site publication of Mackenzie Delta stratigraphy (Murton, et al., 2004) and there are many reports of permafrost geomorphology and coastal processes in the Mackenzie Delta-Beaufort Sea region (e.g. Harper, et al., 1985; Baird, 1995; Taylor, et al., 1996; Solomon, 2005; Couture, et al., 2015).

As Pullen Island lies within the continuous permafrost zone, the ground below a certain depth remains frozen throughout the year. The island has a maximum elevation of 26 m at the top of the west-facing cliffs, and is marked by ice-wedge polygon networks. The upper layer of material that thaws seasonally is termed the active layer; this material is generally thought to be most susceptible to erosion in the summer months (Aré, et al., 2008). The thickness of the active layer is inherently linked to summer temperatures, which affect the depth to which the ground thaws.

Murton et al. (2004) identified two stratigraphic units on Pullen Island, accounting for the upper 16 m; sandy silt and massive ice. The sediment unit is approximately 12 m thick, and includes unlithified sandy silt, fine sand, and few pebbles to cobbles which are interpreted to have been brecciated subglacially at the margin of the Laurentide Ice Sheet, in addition to ice veins and blocks. The massive ice unit is at least 4 m thick, and is interpreted as buried basal ice (Murton, et al., 2004). The contact between the sediment unit and the underlying massive ice is an angular unconformity. Ground ice, as blocks and wedges, is visible in the cliff face. The west-facing cliff has been visually classified as having high ice content (>75%; Couture, et al., 2015).

2.2. Coastline digitization

Drone-based aerial imagery from 2016, 2017 and 2018 was processed using Pix4Dmapper photogrammetry software to produce georeferenced digital surface models (DSMs) and aerial imagery mosaics, georeferenced using ground control points measured during each survey. A DSM was similarly generated using aerial imagery from 1992 and elevation control points based current inland elevations.

A greater temporal extent has been achieved using historical aerial photographs, although at the cost of resolution and positional referencing quality (Table 2). The photographs, obtained from Natural Resources Canada archives, were scanned at 600 dpi and georeferenced in ArcMap. The control points used were primarily located at ice-wedge intersections, referenced to the 2016-2018 imagery.

Coastlines were identified based on slope morphology; the “cliff line” being the upper edge of the slope and the “shoreline” being the base. The lines were digitized by hand in ArcMap for each year with available imagery, and were drawn by a single user for consistency. GPS points from ground surveys of the cliff line in 2013-2015 were converted to lines in ArcMap and compiled with the digitized cliff lines in a single shapefile (Fig. 3). Cliff and shorelines from a total of 13 years spanning 1947-2018, were included in the final calculations (Table 2).

The positional error of each image was measured relative to the imagery for 2018. Because cliff retreat was calculated as the relative change in cliff line position, the error in geographic position is less important to the measurement than error in registration between images. Thus, the error was measured as the distance between the registered location of the same feature on the image in question and the 2018 imagery when the two where overlain in a GIS. Where identifiable on the imagery, 26 points were chosen for validation, which were not used as georeferencing points in the registration of the imagery. Imagery from 1985 had the maximum root mean square (RMS) positional error recorded (7.87 m relative to the 2018 imagery). The coarse resolution and low visual contrast of the 1985 imagery posed a particular challenge when locating control points for georeferencing as fewer landmarks (such as ice-wedge polygons) were visible.

For each year with imagery of sufficient resolution, sections of cliff were visually categorized as *clearly slumping*, *clearly block failure*, or *transitional*. Two areas were isolated for rate comparison; a section of cliff where the primary erosion mechanism is slumping, and a section dominated by block failure (Fig. 3). The cliff retreat rates were calculated for each period using transects that could be used to consistently compare both landward recession and form change through time.

2.3. Cliff retreat rate calculation

The Digital Shoreline Analysis System (DSAS; Theiler, et al., 2017), an extension for ArcMap, was used to calculate the rates of cliff line change. DSAS requires the user to input digitized cliff lines, over which transects are drawn from a user-defined baseline every 10 m. The system computes the distance between each point along a transect where it is intersected by a cliff line, and the positional difference between successive cliff lines can then be converted to mean annual retreat rates by dividing by the number of years between the two points. The mean rate was calculated for each pair of cliff-lines, and the mean annual values were used as the short-term rates. Three equal-interval periods (1947-1970, 1971-1994, and 1995-2018) were used for long-term rates calculations. Standard deviations have been calculated for each of the determined rates to represent the spatial variation occurring during each time period.

2.4. Volume change calculation

Volume change within the block failure and slump areas (Fig. 3) were calculated based on elevation differences of DSMs from 1992, 2016, 2017, and 2018. Positive and negative volume changes were calculated separately to differentiate areas of accretion or erosion of material, and then combined to find the net volume change. Values are reported as mean annual change in m^3 per 100 m of shoreline in the later year of the timestep (i.e., for 2017-2018, the length of the 2018 shoreline is used).

2.5. Air temperature and storms

Landfast ice (immobile sea ice that is fixed to the coast; Mahoney, 2018) has historically been present in the region between February and June in the Mackenzie Delta region, and there appears to be a trend of later onset of landfast ice formation by approximately 2.80 weeks per decade (mean formation and breakup for 1983-2009; Galley, et al., 2012). Considering the presence of pack ice, the traditional open water seasons have typically been between July and September (Solomon, 2005). The presence of sea ice up to the shore limits thermal erosion by wave action, so analysis was restricted to the open water season (Aré, et al., 2008; Wobus, et al., 2011). For this analysis, the open water season for inclusion of storm events was maintained as July to September, however it should be noted that some events outside of this period that could have impacted coastal retreat rates may have been excluded in the case of longer open water periods in a given year.

Wind and air temperature data from the Environment and Climate Change Canada weather station in Tuktoyaktuk, N.W.T., for the 1958-2018 open water seasons (July, August, and September) were processed using methods adapted from Atkinson (2005). Data were collected every 6 hours between 1958 and 1992, and hourly between 1993 and 2018. The dataset occasional gaps of ≤ 5 hours, approximately 30 gaps of 6 – 24 hours, and 8 gaps of > 24 hours. The missing times were excluded from the analysis, although we acknowledge that this may have resulted in missed or underestimated duration of storm events due to broken continuity of the record.

Storms were defined as events with wind speeds of at least 10 m s^{-1} sustained over at least 6 hours. These were filtered for events which would affect the actively eroding side of Pullen Island; storms with onshore wind directions between 270º and 15º from the north. “Synoptic duration” was calculated as the time between the first and last recorded wind speeds exceeding 10 m s^{-1} for each event. “Core duration” was calculated as the time during which wind speed was in the upper 50th percentile for each event. An example of the threshold wind speeds for a single event are shown in Fig. 4 to illustrate the definition of these storm duration values. The average synoptic and core durations and the mean air temperature have been calculated for every year on record. A 5-year moving average was calculated for each metric, and linear regressions (date against storm duration and date against temperature) were calculated using these averages to assess weather trends over the period of observation.

Satisfaction of the assumptions of linear regression was assessed for each of the dependent variables (cliff retreat across the study area, in the block failure area, and in the slump area) and independent variables (air temperature and core storm duration). Observations are independent from one another; the values used for each data point represent discrete periods of time. The independent variables are normally distributed. Although the the rates of cliff retreat in the slump area and over the entire study area are moderately left-skewed and the rates of retreat in the block failure area are severely right-skewed (skew coefficient of 1.3), the regressions do not exhibit heteroscedasticity when residuals are plotted against predicted values. As such, linear regression is considered acceptable for our purposes.

The mean cliff retreat rates for the entire study area and for each of the block failure and slump areas were regressed against mean air temperature and mean core storm duration. For this calculation, the mean weather metrics for the entire time step was compared to the annual rate of retreat. For example, the mean air temperature for all of 1967 to 1974 was used as the x-value to the mean retreat rate in the slump area for this period. Similar regressions were also calculated for mean air temperature and mean core duration against the mean retreat in the entire study area. For each regression, coefficients of determination (r^2) and probability values (p) were calculated, to comment on the significance of the observed relationships. Note that because weather data begin at 1958 and the next available imagery was from 1967, the first time interval for the long-term comparison only represents the step from the 1967 to 1974 imagery.

3. Results

The mean annual rate of cliff retreat, calculated over the entire study area, shows a three-phase increase: rising by 0.53 m a^{-1} $decade^{-1}$ (1947 – 1985), through 1.8 m a^{-1} $decade^{-1}$ (1985 – 2013) to an increase of 1.6 m a^{-2} (2013 – 2018; Fig. 5 A). The range of rates experienced across the study area also increased over time (Fig. 5 B). Certain areas, such as the west facing cliff section, maintained a more consistent rate of change throughout the study period, while others experienced more dramatic increases in cliff retreat rates (Fig. 6). The mean retreat rates were broken down into two categories based on failure mechanism, namely: “block failure” areas and “slump” failure areas (Fig. 5 C). While equal within one standard deviation to the mean cliff retreat rates for the corresponding time period, shoreline retreat rates show a more gradual trend over time: decreasing slightly by 0.15 m $a^{-1}$$decade^{-1}$ (1947-1985), then rising by 1.2 m a^{-1} $decade^{-1}$ (1985-2004), followed by 3.9 m a^{-1} $decade^{-1}$ (2004-2018; Fig. 5 D). There was an overall increase in range of shoreline retreat rates across the study area (Fig. 5 E, however when divided by failure mechanism the area experiencing block failure remained more consistent through time, while the greatest change was in areas experiencing slumping (Fig. 5 F).

The mean annual volume change per 100 m of shoreline for each period (1992-2016, 2016-2017, 2017-2018), in each of the block failure and slump areas, is shown along with the mean rates of cliff and shoreline retreat (Fig. 8). Volume change over all time steps was greater in the slump area than the block failure area by an order of magnitude, however the same pattern is shown in both cases; the greatest change is seen over the 2016-2017 period.

The mean air temperature for July, August, and September recorded at Tuktoyaktuk has been calculated for each year between 1958 and 2018, in addition to a 5-year moving average. There is an increasing trend of 3°C per century (Fig. 9A), with annual variations within ±3°C of the trendline. Regressions of mean air temperature against rate of cliff retreat (Fig. 9B) reveal a positive, although statistically insignificant correlation across the entire study area ($r^2 = 0.34$; $p = 0.08$), in areas dominated by block failure ($r^2 = 0.08$; $p = 0.5$), and areas dominated by slumping ($r^2 = 0.41$; $p = 0.05$).

The mean annual synoptic and core duration of storms has been identified for the period between 1958 and 2018 (Fig. 9C). Regressions of mean core storm duration against rate of cliff retreat were calculated (Fig. 9D). Positive, but statistically insignificant relationships were found across the entire study area ($r^2 = 0.13$; $p = 0.3$) and in areas dominated by slumping ($r^2 = 0.34$; $p = 0.08$). There is a statistically significant relationship between core storm duration and cliff retreat in the block failure area ($r^2 = 0.84$; $p = 0.0002$).

4. Discussion

The observed rates of cliff and shoreline retreat on Pullen Island (3.4 ± 2.7 m a^{-1} and 2.3 ± 3.0 m a^{-1}, respectively) was within one standard deviation of the value of coastal retreat reported by Solomon (2005; see Table 1) for the outer Mackenzie Delta islands (1.5 ± 2.8 m a^{-1}) during comparable time periods (1974-2004 and 1972-2000). Over the entire period of observation (1947-2018), the northwest-facing sections of cliff experienced the most retreat, having lost as much as 330 m over this period and experiencing rates of cliff retreat up to 30 m a^{-1} in some areas. The mean annual rate over the whole study area has increased from 0 to 12 m a^{-1}. The increase in activity is not uniform across the entire cliff, however; the most change is seen around the RTS features, which experienced over 20 m a^{-1} headwall retreat in 2013-2018. Rates of retreat have also increased, although to a lesser degree, in both the non-retrogressive slump sections and block-failure sections (Fig. 6). Indeed, the long-term rates of cliff retreat in the block failure areas and areas of non-retrogressive slumping were primarily between 0 and 5 m a^{-1} between 1947 and 1993. In the following period, 1994-2018, the cliff sections were more variable with regard to rate of retreat; the standard deviation of retreat increased from 3.8 m a^{-1} to 6.5 m a^{-1}.

The correlations between retreat rate and both air temperature and core storm duration suggest that both have an influence on cliff retreat; this is in agreement with previous studies relating Arctic coastal erosion to these parameters, including Solomon, et al. (1994), who found that storm intensity was positively correlated with cliff retreat near Tuktoyaktuk and along the Yukon coast, and Günther, et al. (2015), who found that summer air temperature was positively correlated with cliff retreat on the Laptev Sea coast. Furthermore, we find that the impacts of air temperature and storm duration seem to have a greater or lesser effect depending on the dominant mechanism of erosion. It appears that warmer years see more cliff retreat, and more so in the slump areas than block failures. Similarly, years with longer duration of storms tend to experience more cliff retreat, and more so in the areas affected by block failures. This also suggests that, on a broad spatial scale, the decrease in homogeneity of retreat rate appears to be related to different magnitudes of response to environmental change, depending on the primary mechanism of cliff failure for a particular segment of coast.

4.1. Block failure responses

Block failure accounts for a small but annually increasing section of west-facing cliff. It occurs when the base of the cliff is undercut by waves and thermal erosion, and a whole block of material detaches from the cliff face due to lack of underlying support (Wobus, et al., 2011). The occurrence of block failure can be related primarily to the strength and frequency of storms (Baird 1995), which cause the surges that remove cliff-base sediment and induce thermal erosion at the cliff base. These erosion processes are limited to the open-water season, when sea ice has melted such that waves form and reach the cliff (Aré, et al., 2008; Wobus, et al., 2011). The two weather components assessed, summer air temperature and storm duration, have positive correlations with block failure. Warmer years are likely to have longer open-water seasons (Goegh-Guldberg, et al., 2018), and so have longer periods over which storms may generate waves to cause block failure.

Given the multi-year frequency and variable resolutions of imagery used, assessment of the relationship between weather and cliff retreat assumes that the mean trend effectively represents the mean annual trend. For example, the average number of storms over the time interval represented by the gap between images correlates with the mean retreat rate for that period. However, for much of the study period it cannot be established whether erosion during the survey-dependent time intervals occurred in the year with the most storms. Cliff change data at the annual resolution are only available for 2016-2018. Over this limited period, however, it was found that the three storms identified between 2016 and 2017 observations had longer core durations and faster wind speeds than the four storms between 2017 and 2018 observations, and that more cliff was lost in the block failure area in the 2016-2017 season. The long-term increasing trends in both summer air temperature and core storm duration suggest that there will be a continued increase in rate of cliff retreat in the block failure areas in the future.

4.2. Slump failure responses

The majority of the surveyed cliff area is eroded primarily through slumping failures, which in permafrost coasts is driven by ground ice melt. This releases previously-frozen sediment, removes support for overlying material, and entrains material as the meltwater runs downslope. Generally, the amount of melt depends on the net solar radiation that is received by the ground ice (Lewkowicz, 1986). The high latitude and well-constrained study area means that: (a) air temperature is an acceptable generic proxy for solar input, and (b) differences in melt are due to locally-defined slope angle and ice exposure, both of which impact net radiation. Theoretically, higher air temperatures would result in more melt, and thus more rapid headwall retreat; this is supported by the positive correlation between retreat rate and air temperature (Fig. 9 B).

There is notable heterogeneity of cliff retreat rates within areas of apparently similar erosion mechanisms, so lateral structural variations must also be considered. The most obvious distinction is between areas with RTS and those without. Along the northern-most cliffs, slumping occurs, but there is no development of discrete RTS features. In the central cliff section there are two large, pervasive RTS failures that can be tracked through the study period. The first is currently stable, but over the course of the study period has exhibited several periods of accelerated activity (some time prior to 1947, and for an unknown period between 1992 and 2013 that included 2004) and quiescence (between 1967 and 1985, and again around 2013). The second appears to have initiated around 2013 along the same slope as the former RTS, and retrogressed sufficiently to overtake the original headwall. This "polycyclic" RTS activity, where new slumps initiate on top of older, stabilized slumps, is observed elsewhere in the Beaufort Sea (Lantuit & Pollard, 2008). In the transitional and block failure areas small, recurring RTS have also been observed, which we will refer to as *perennial*, because they develop year after year on the same ice block but do not persist between melt seasons. This is in contrast to the large, *annual* RTS, which persist between melt seasons and thus can progress further from the headwall position attained the previous year.

The relationship between headwall retreat of an active RTS and meteorological data has been documented in regions near Pullen Island; there is a direct correlation between ablation of exposed ground ice and air temperature (Lewkowicz, 1986). Furthermore, there are several known factors which contribute to RTS initiation and maintenance of activity (or, inhibition of stabilization), including size of ice body, slope and ice face angles, and cliff height (Lewkowicz, 1986; 1987). Overall, the most important condition of continued RTS activity is that the ice remain exposed; if it becomes covered by sediment due to insufficient slope or melt to remove it, or if the ice body is exhausted, then activity will cease (Burn & Lewkowicz, 1990). Exposed ground ice appears to be primarily wedge ice formations, due to the lateral continuity between the ice and the network of polygon on the ground surface. Ice wedge polygon density on the surface appears fairly uniform over the whole slump area, so the lateral differences may cause some variation, but would likely even out over longer time scales.

Slope angle is generally steeper outside of RTS structures, however this is interpreted as a result of the slumps, and not their cause. Based on elevation models, it appears that the slope angle within an RTS reclines over time, while the slumping coastal cliffs maintain a more consistent slope angle (Fig. 10). Exposed ground ice has been observed throughout the study area, raising questions over why certain areas develop annual RTS structures, while other areas (with apparently similar structural characteristics and external forces) do not. There are two factors to consider that may play a large role in deciding the development of an RTS; cliff height, and adjacent cliff behavior.

Broadly speaking, ground materials that are mobilized downslope in an RTS system may come to rest on the headwall, accumulate on the slump floor, or enter the nearshore sediment budget. Lewkowicz (1987) attributed differences in sediment removal to headwall elevation; lower headwalls are more likely to have their ice covered by sediment, impeding ice ablation and halting thaw-related slumping. This is further supported by Ramage, et al. (2017), who found that coastal RTS activity on the Yukon coast was more likely to occur in areas with higher, steeper cliffs compared to lower or shallower slopes. In the context of our study area, the highest headwall elevations are found in the RTS area, with median elevation 23.5 m. This is followed by the non-RTS slump area, which has a median headwall elevation of 18 m. Finally, the block failure area has median headwall elevation of 6 m. A possible interpretation is that RTS structures developing in the block failure area tend to have their ice covered efficiently by sediment and subsequently cease activity. Perennial RTS are observed in the block failure area over successive years, but the adjacent cliff is retreating at such a rate that the characteristic bowl structure is removed before the end of the melt season and loses the positive feedbacks of increased surface area on ablation rate (Lacelle, et al., 2015). One determining parameter of the development of an annual RTS feature is sufficient activity to sustain a more rapid rate of retreat than the adjacent cliff sections. It is perhaps only necessary to maintain this localized elevated rate for a single melt season, such as to establish a bowl-shaped structure of sufficient size that will then begin the following melt season with higher retreat rates than the adjacent cliff. Due to the temporal resolution of the data, this cannot be confirmed for the identified annual RTS. Given the polycyclic nature of RTS, observed on Pullen Island and elsewhere in coastal (Lantuit & Pollard, 2008) and lakeside (Kokelj, et al., 2009) settings, one predictor of RTS activity is prior RTS activity in the region. Considering the history of the study area through the available imagery, it is unlikely that annual RTS structures such as those seen in the slump area will develop in the block failure area.

4.3 Alternative coastal change measurements: Shoreline retreat and volume change

Measurements of mean annual retreat of the shoreline (defined here as the base of the slope) yielded similar trends to cliff retreat, being equal within one standard deviation and following the increase in rate over time, although to a lesser degree until the latest period of acceleration (Fig. 5). This would suggest that using either the shore or the cliff line give an adequate broad sense of coastal change through time, but that at the annual resolution are somewhat disconnected from one another, and from measures of volumetric change.

A preliminary statement about the link between shoreline, cliff line, and volumetric changes can be made based on the four DSMs included in this analysis (1992, 2016, 2017, 2018). When the volumetric change over the block failure and slump areas were calculated from elevation difference between consecutive DSMs, it appears that volume is more directly related to retreat in the block failure area than in the slump area. In the area dominated by block failure, years of greater cliff and shoreline retreat also have greater volume of material lost. In the area affected by slumping, the pattern of volume loss tracks more closely with retreat of the cliff line, while there appears to be a disconnect between volume loss and shoreline retreat; the greatest mean annual volume change of the three periods occurred in 2016-2017, while the greatest shoreline retreat occurred in 2017-2018 (Fig. 8).

One potential explanation for the disconnect between shoreline, cliff line, and volume changes are the pathways for eroded material depending on the dominant erosive mechanism. Obu, et al. (2016), observed that within their study area on Herschel Island, Yukon, volumetric change was more laterally uniform than planimetric measurements of coastal change, and that some of the short term variability in coastal retreat was related to lag between detachment of material from the slope and removal from the shore. In areas being eroded by block failure, material is detached simultaneously from the cliff edge and observable slope base, then removed to the nearshore environment over a period of a couple weeks (Barnhart, et al., 2014). It follows, therefore, that planimetric measures of coastal change and loss of material would follow similar trends.

Where the cliff is being eroded by slumping, material is not removed simultaneously from the cliff edge and slope base; sediments may be deposited on the slope, in the base of an RTS, or at the base of the slope, before being removed to the nearshore. Indeed, some net accumulation of sediments is observed within the active RTS in 2016-2017 and 2017-2018 (Fig. 7 B & C; up to 3 m surface elevation increase). Discrepancies between the amount of material removed from the cliff and from the shore may be the result of redeposition prior to reaching the shore (Obu, et al., 2016), volume change due to ice melt (Couture, et al., 2018), or due to short-term inconsistencies related to the processes driving sediment movement on the cliff edge (i.e. gravity-driven mobilization) and the slope base (i.e. wave action).

The connections drawn here between volume change and cliff and shoreline retreat on Pullen Island are preliminary due to the inclusion of only three time periods in the analysis. There is some suggestion in the literature that over sub-annual period there would be more disconnect between cliff and shoreline change, which tend to equilibrate over the course of one or more seasons (Barnhart, et al., 2014). The appropriate metric of coastal change likely depends on the application of this value. Net change in volume may be the most representative, if not the most intuitive metric to apply practically. Adjusting volumetric measurements to account for ice content, thus reporting the change in sediment volume, has been applied to studies of mobilization of carbon, nitrogen, and other soil constituents and impacts on the marine environment (e.g., Couture, et al., 2018; Ramage, et al., 2018). Changes to shoreline is a commonly used value, and similarly relates to the nearshore sediment budget (e.g., Harper, 1978; Solomon, 2005). However, for applications regarding terrain loss, impacting terrestrial ecosystems and human land-use and infrastructure, cliff retreat appears to be the most intuitive measurement to report, especially considering the increaing RTS activity across the Canadian Beaufort Sea Coast, and the potential for discrepancy between cliff and shoreline retreat over short periods of time.

4.4 Other explanators of coastal retreat

The stratigraphy of Pullen Island is one of the most important factors controlling how rapidly the cliffs are eroding, and their response to other environmental drivers. The ice fraction of eroded material melts and does not become redeposited (Harper, et al. 1985), which contributes to the extreme rates of cliff retreat experienced in this area compared to non-permafrost coasts. Limiting sediment as talus prolongs ice exposure and increases local relief (Kokelj, et al., 2015; Aré, 1988), and leaves the cliff base exposed to thermal and mechanical abrasion (Baird, 1995; Aré, 1988).

Slope aspect may also impact cliff retreat as it relates to insolation, which provides the energy to thaw the active layer and sustain RTS activity (Lewkowicz, 1986). Variations in aspect within the study area can result in local differences in net radiation (Lewkowicz, 1986; 1987). The eroding coasts on Pullen Island range from north-facing in the north of the study area, to west-facing in the south of the study area. Being in the northern hemisphere, the more west-facing slope will receive more direct solar radiation than the north-facing region. However, it is noted that the diffuse sunlight at this latitude and extended polar day mean that the impact is likely not very large compared to other factors which drive coastal retreat (Wobus, et al., 2011; Aré, 1988). Nonetheless, variation in slope aspect may help to explain, at least in part, the lateral differences in retreat rate of the slumping coastal cliffs in the later years of observation (Fig. 6).

The relationship between failure, transport, and deposition in the nearshore environment is somewhat iterative. The amount of failure determines the volume available to be deposited; this volume decreases when the ice fraction melts. The volume deposited at the base of the slope in turn affects the amount of erosion; where there is less sediment available to protect the base of the slope, more rapid removal of material should occur. The balance is maintained by ice content and slope, which influence effective transport; however, these variables are also dependent on the mechanisms of failure and deposition. Changes to one or more of these factors, such as increased air temperatures resulting in more melt or longer open-water seasons and hence the susceptibility to wave action, resulting in a change to the other processes in the cycle. While the finer nuances of these relationships are beyond the scope of this paper, the movement of material and the characteristics (ice content, cliff height, air temperature, etc.) of the local environment in which it takes place are essential and interdependent controls on the rate of retreat of ice rich permafrost cliffs.

5. Conclusions

The rate and variability of retreat across the ice-rich cliffs of Pullen Island have increased over the 71 years of observation; the island has gone from a mean annual retreat of < 1 m with standard deviation of 2.1 during the 1940s to 1980s, to 12 m a^{-1} retreat with standard deviation of 6.3 in the final five years of the study. The acceleration in retreat is interpreted primarily as response to increasing air temperatures causing increased ground ice melt. The magnitude of response to air temperature change depends on the dominant erosive mechanism for a particular section of cliff; the slump-dominated cliffs, specifically around the RTS features, accelerated faster than the block failure-dominated sections. The decreasing uniformity of cliff retreat is expected to continue in response to current air temperature trends.

Between 1947 and 2018, Pullen Island experienced cliff line retreat of up to 330 m in some areas, of which up to 50 m retreat occurred between 2013 and 2018. In 2018, the width of the island was approximately 550 m behind the more slowly eroding areas, and between 250 m and 500 m behind the more rapidly eroding areas. If the current retreat rate of 12 m a^{-1} is sustained, Pullen Island will cease to exist in its currently recognizable form by the year 2060. Considering the acceleration of retreat that is experienced, however, this may come ten or fifteen years sooner, given the mean long-term acceleration of 0.2 m a^{-1} since 1947, or that of 1.6 m a^{-1} seen between 2013 and 2018.

Both shoreline and cliff line reatreat rates are used as measures of coastal change thoughout the literature, However, the short-term disconnect between the two metrics may be exacerbated by increased slump activity in the Mackenzie Delta region (Couture, et al., 2015; Barnhart, et al., 2014). The respective implacations for marine and terrestrial impacts of shoreline or cliff line change rates suggests that care should be taken to report the appropriate values depending on their intended application. Where issues of terrain loss are concerned, cliff line retreat appears to be the more intuitive and useful metric of coastal change.

As noted, these conclusions are based on trends of multi-year averages. Future work in this area, with a greater frequency of measurements allowing for annual resolution, will be required to better understand the strength of the relationship between the mechanisms driving cliff retreat and environmental factors. Nevertheless, it is apparent that mechanism-specific magnitudes of response to environmental change contributes to the dynamic complexities of permafrost cliff systems.

Acknowledgement

Funding and support for this project was provided by Natural Resources Canada through the Climate Change Geoscience Program and Polar Continental Shelf Project (PCSP). Additional funding was provided by the Inuvialuit Regional Corporation (IRC) and Crown-Indigenous Relations and Northern Affairs Canada (CIRNAC) through the Beaufort Sea Regional Strategic Environment and Research Assessment (BRSEA). In addition, this work was made possible through the Natural Environment and Research Council (NERC) sponsored UK-Canada Arctic bursary program. We are grateful to the field crews, in particular Paul Fraser, Angus Robertson, Roger Macleod from NRCan and Andrew Clark from the University of Calgary for acquiring the UAV data used in this study. We would also like to acknowledge the Aurora Research Institute (ARI), the Inuvialuit Game Council, and the communities and Hunters and Trappers Committees of Inuvik and Tuktoyaktuk for their continued support.

References

Aré, F. E., 1988. Thermal abrasion of sea coasts (part I). Polar Geography and Geology, 12(1), p. 1.

Aré, F., Reimnitz, E., Grigoriev, M., Hubberten, H.-W., & Rachold, V., 2008. The influence of cryogenic processes on the erosional Arctic shoreface. Journal of Coastal Research, 24(1), pp. 110-121.

Atkinson, D. E., 2005. Observed storminess patterns and trends in the circum-Arctic coastal regime. Geo-Marine Letters, 25(2), pp. 98-109.

Baird, W. F., 1995. Thermal-mechanical model for erosion processes on Arctic coasts, s.l.: s.n.

Barnhart, K. R., Anderson, R. S., Overeem, I., Wobus, C., Clow, G. D., Urban, F. E., 2014. Modeling erosion of ice-rich permafrost bluffs along the Alaskan Beaufort Sea coast. Journal of Geophysical Research: Earth Surface, 119, doi: 10.1002/2013JF002845

Boak, E. H., Turner, I. L., 2005. Shoreline definition and detection: A review. Journal of Coastal Research. 214, pp. 688-703. doi: 10.2112/03-0071.1

Burn, C. R. & Lewkowicz, A. G., 1990. Retrogressive thaw slumps. The Canadian Geographer, Volume 34, pp. 273-276.

Cassidy, A. E., Christen, A., Henry, G. H. R., 2016. The effect of a permafrost disturbance on growing-season carbon dioxide fluxes in a high Arctic tundra ecosystem. Journal of Geophysical Research: Biogeosciences, 13, pp. 2291-230. doi: 10.5194/bg-13-2291-2016

Cunliffe, A. M., Tanski, G., Radosavljevic, B., Palmer, W. F., Sachs, T., Lantuit, H., Kerby, J. T., Myers-Smith, I. H., 2019. Rapid retreat of permafrost coastline observed with aerial drone photogrammetry. The Cryosphere, 13, pp. 1513-1528. doi: 10.5194/tc-13-1513-2019

Couture, N. J., Forbes, D. L., Fraser, P. R., Frobel, D., Jenner, K. A., Manson, G. K., Solomon, S. M., Szlavko, B., Taylor, R. B., 2015. A coastal information system for the southeastern Beaufort Sea, Yukon and Northwest Territories. Geological Survey of Canada Open File 7778.

Couture, N. J., Irrgang, A., Pollard, W., Lantuit, H., Fritz, M., 2018. Coastal erosion of permafrost soils along the Yukon Coastal Plain and fluxes of organic carbon to the Canadian Beaufort Sea. Journal of Geophysical Research: Biogeosciences, 123(2), pp. 406-422. doi: 10.1002/2017JG004166

Dallimore, S. R., Wolfe, S. A., Solomon, S. M., 1996. Influence of ground ice and permafrost on coastal evolution, Richards Island, Beaufort Sea coast, N.W.T. Canadian Jounral of Earth Sciences, 33, pp.664-675.

Environment Canada, 2014. Coastal and nearshore bird usage of the Canadian Beaufort Sea. Data prepared by the Canadian Wildlife Service (CWS) and Upon-LGL Limited.

Goegh-Guldberg, O. D., Jacob, D., Taylor, M., Bindi, M., Brown, S., Camilloni, I., Diedhiou, A., Djalante, R., Ebi, K. L., Engelbrecht, F., Guiot, J., Hijioka, Y., Mehrotra, S., Payne, A., Seneviratne, S. I., Thomas, A., Warren, R., Zhou, G. 2018. Impacts of 1.5ºC global warming on natural and human systems. In: V. Masson-Delmotte, V., Zhai, P., Portner, H.-O., Roberts, D., Skea, J., Shukla, R. P., Pirani, A., Moufouma-Okia, W., Pean, C., Pidock, R., Connors, S., Matthews, J. B. R., Chen, Y., Zhou, X., Gomis, M. I., Lonnoy, E., Maycock, T., Tignor, M., Waterfield, T. eds. Global warming of 1.5ºC. An IPCC Special Report on the impacts of global warming of 1.5ºC above pre-industrial levels and related global greenhouse gas emission pathways, in the context of strengthening the global response to the threat of climate change, sustainable development, and efforts to eradicate poverty.

Günther, F., Overduin, P. P., Yakshina, I. A., Opel, T., Baranskaya, A. V., Grigoriev, M. N., 2015. Observing Muostakh disappear: permafrost thaw subsidence and erosion of a ground-ice-rich island in reponse to arctic summer warming and sea ice reduction. The Cryosphere, 9(1), pp. 151-178. doi: 10.5194/tc-9-151-2015

Harper, J. R., 1978. Coastal erosion rates along the Chukchi Sea coast near Barrow, Alaska. Arctic, 31(4), pp. 428-433.

Harper, J. R., 1990. Morphology of the Canadian Beaufort Sea Coast. In: P. R. Hill, ed. The Beaufort Sea coastal zone. Marine Geology, pp. 75-91.

Harper, J. R., Reimer, P. D., Collins, A. D., 1985. Canadian Beaufort Sea: Physical shore-zone analysis. Geological Survey of Canada Open File 1689.

Hugelius, G., Strauss, J., Zubrzycki, S., Harden, J. W., Schuur, E. A. G., Ping, C.-L., Grosse, G., Michaelson, G. J., Koven, C. D., O'Donnell, J. A., Elberling, B., Mishra, U., Camill, P., Yu, Z., Palmtag, J., Kuhry, J. A. 2014. Estimated stocks of circumpolar permafrost carbon with quantified uncertainty ranges and identified data gaps. Journal of Geophysical Research: Biogeosciences, 11, pp. 6573-6593. doi: 10.5194/bg-11-6573-2014

Kokelj, S. V., & GeoNorth Ltd., 2002. Drilling mud sumps in the Mackenzie Delta Region: Construction, abandonment and past performance. Report to the Department of Indian Affairs and Northern Development, Northwest Territories Region. 16 p.

Kokelj, S. V., Lantz, T.C., Kanigan, J., Smith, S.L., Coutts, R. 2009a. Origin and polycyclic behaviour of tundra thaw slumps, Mackenzie Delta region, Northwest Territories, Canada. Permafrost and Periglacial Processes, 20(2), pp. 173-184.

Kokelj, S. V., Zaidlik, B., Thompson, M. S. 2009b. The impacts of thawing permafrost on the chmistry of lakes across the subarctic boreal-tundra transition, Mackenzie Delta region, Canada. Permafrost and Periglacial Processes, 20, pp. 185-199. doi: 10.1002/ppp.641

Kokelj, S. V., Tunnicliffe, J., Lacelle, D., Lantz, T.C., Chin, K.S., Fraser, R. 2015. Increased precipitation drives mega slump development and destabilization of ice-rich permafrost terrain, northwest Canada. Global and Planetary Change, Volume 129, pp. 56-68.

Lacelle, D., Brooker, A., Fraser, R. H., Kokelj, S. V., 2015. Distribution and growth of thaw slumps in the Richardson Mountains-Peel Plateau region, northwestern Canada. Geomorphology, Volume 235, pp. 40-51.

Lantuit, H. & Pollard, W. H., 2005. Temporal stereogrammetric analysis of retrogressive thaw slumps on Herschel Island, Yukon Territory. Natural Hazards and Earth Systems Sciences, 5, pp. 413-423.

Lantuit, H. & Pollard, W. H., 2008. Fifty years of coastal erosion and retrogressive thaw slump activity on Herschel Island, Southern Beaufort Sea, Yukon Territory, Canada. Geomorphology, 95(1), pp. 84-102.

Lewkowicz, A. G., 1986. Rate of short-term ablation of exposed ground ice, Banks Island, Northwest Territories, Canada. Journal of Glaciology, 32(112), pp. 511-519.

Lewkowicz, A. G., 1987. Headwall retreat of ground-ice slumps, Banks Island, Northwest Territories. Canadian Journal of Earth Science, Volume 24, pp. 1077-1087.

Mackay, J. R., 1986. Fifty years of coastal retreat west of Tuktoyaktuk, District of Mackenzie. Current Research, Part A, Geological Survey of Canada, Paper 86-1A, pp. 727-735. doi: 10.4095/120445

Mackay, J. R., 1972. The world of underground ice. Annals of the Association of American Geographers, 62(1), pp. 1-22. doi: 10.1111/j.1467-8306.1972.tb00839.x

Manson, G. K. & Solomon, S. M., 2007. Past and future forcing of Beaufort Sea coastal change. Atmosphere-Ocean, 45(2), pp. 107-122.

Murton, J. B., Waller, R. I., Hart, J. K., Whiteman, C. A., Pollard, W. H., Clark, I. D. 2004. Stratigraphy and glaciotectonic structures of permafrost deformed beneath the northwest margin of the Laurentide Ice Sheet, Tuktoyaktuk Coastlands, Canada. Journal of Glaciology, 50(170), pp. 399-412.

Obu, J., Lantuit, H., Fritz, M., Pollard, W. H., Sachs, T., Günther, F., 2016. Relation between planimetric and volumetric measurements of permafrost coast erosion: a case study from Herschel Island, western Canadian Arctic. Polar Research, 35(1), 30313, doi: 10.3402/polar.v35.30313

Rachold, V., Grigoriev, M. N., Aré, F. E., Solomon, S., Reimnitz, E., Kassens, H., Antonow, M, 2000. Coastal erosion vs riverine sediment discharge in the Arctic Shelf seas. International Journal of Earth Sciences, 89(3), pp. 450-460.

Radosavljevic, B., Lantuit, H., Pollard, W., Overduin, P., Couture, N., Sachs, T., Helm, V., Fritz, M., 2016. Erosion and flooding - threats to coastal infrastructure in the Arctic: A case study from Herschel Island, Yukon Territory, Canada. Estuaries and Coasts, 39(4), pp. 900-915.

Ramage, J. L., Irrgang, A. M., Herzchuh, U., Morgerstern, A., Couture, N., Lantuit, H. 2017. Terrain controls on the occurrence of coastal retrogressive thaw slumps along the Yukon Coast, Canada. Journal of Geophysical Research: Earth Surface, 122, pp. 1619-1634. doi: 10.1002/2017JF004231

Ramage, J. L., Irrgang, A. M., Morgerstern, A., Couture, N., Lantuit, H., 2018. Increasing coastal slump activity impacts the release of sediment and organic carbon into the Arctic Ocean. Journal of Geophysical Research: Biogeosciences, 15, pp. 1483-1495. doi: 10.5194/bg-15-1483-2018

Solomon, S. M., 2005. Spatial and temporal variability of shoreline change in the Beaufort-Mackenzie region, Northwest Territories, Canada. Geo-Marine Letters, Volume 25, pp. 127-137.

Solomon, S. M., Forbes, D. L., Kierstead, B., 1994. Coastal impacts of climate change: Beaufort Sea erosion study. Geological Sruvey of Canada, Open File 2890, 85 p. doi: 10.4095/194148

Statistics Canada, 2016a. 2016 Census – Boundary files: Lakes and rivers (polygons), cartographic boundary file [shapefile]. Statistics Canada Catalogue.

Statistics Canada, 2016b. 2016 Census – Boundary files: Provinces/territories, water file [shapefile]. Statistics Canada Catalogue.

Tanski, G., Lantuit, H., Ruttor, S., Knoblauch, C., Radosavljevic, B., Strauss, J., Wolter, J., Irrgang, A. M., Ramage, J., Fritz, M., 2017. Transformation of terrestrial organic matter along thermokarst-affected permafrost coasts in the Arctic. Science of the Total Environment, 581, pp. 434-447. doi: 10.1016/j.scitotenv.2016.12.152

Taylor, A. E., Dallimore, S. R., Judge, A. S., 1996. Late Quaternary history of the Mackenzie-Beaufort region, Arctic Canada, from modelling of permafrost temperatures. 2. The Mackenzie Delta - Tuktoyaktuk Coastlands. Canadian Journal of Earth Science, 33(1), pp. 62-71.

Thieler, E. R., Himmelstoss, E. A., Zichichi, J. L., Ergul, A., 2017. The Digital Shoreline Analysis System (DSAS) Version 4.0 - An ArcGIS extension for calculating shoreline change. U.S. Geological Survey Open-File Report 2008-1278.

Wobus, C., Anderson, R., Overeem, I., Matell, N., Clow, G., Urban, F. 2011. Thermal erosion of a permafrost coastline: Improving process based models using time-lapse photography. Arctic, Antarctic, and Alpine Research, 43(3), pp. 474-484.

Long-term ice-rich permafrost coast sensitivity to air temperatures and storm influence: lessons from Pullen Island, N.W.T.

H. Bay Berry [a b], Dustin Whalen [a], Michael Lim [c]

[a] Geological Survey of Canada, Bedford Institute of Oceanography, 1 Challenger Drive, Dartmouth, Nova Scotia B2Y 4A2, Canada

[b] Dalhousie University, Department of Earth Sciences, 1459 Oxford Street, Halifax, Nova Scotia B3H 4R2, Canada

[c] Northumbria University, Engineering and Environment, Ellsion Building, Northumberland Road, Newcastle upon Tyne NE1 8ST, UK

Abstract

Response of erosive mechanisms to climate change is of mounting concern on Beaufort Sea coasts, which experience some of the highest erosion rates in the Arctic. Collapse of intact permafrost blocks and slumping within sprawling retrogressive thaw complexes are two predominant mechanisms that manifest as cliff retreat in this region. Using aerial imagery and ground survey data from Pullen Island, N.W.T., Canada, from 13 time points between 1947 and 2018, we observe increasing mean retreat rates from 0 $\pm$ 4.8 m/a in 1947 to 12 $\pm$ 0.3 m/a in 2018. Mean summer air temperature was positively correlated with cliff retreat over each time step via block failure (r^2 = 0.08; p = 0.5) and slumping (r^2 = 0.41; p = 0.05), as was mean storm duration with cliff retreat via block failure (r^2 = 0.84; p = 0.0002) and slumping (r^2 = 0.34; p = 0.08). These data indicate that air temperature has a greater impact in slump-dominated areas, while storm duration has greater control in areas of block failure. Increasingly heterogeneous cliff retreat rates are likely resulting from different magnitudes of response to climate trends depending on mechanism, and on geomorphological variations that prescribe occurrences of retrogressive thaw slumps.

Key words: coastal erosion, permafrost, slope instability, arctic climate change.

1. Introduction

The ice-rich nature of the Beaufort Sea permafrost coasts has contributed to widespread, rapid coastal retreat. Even with the processes which drive erosion in this setting being restricted to the few open-water months each year (Aré, et al., 2008), the reported mean coastal retreat rate for most areas of the Canadian Beaufort Sea in the late 20th and early 21st century was 1 m a^{-1}, with some locations experiencing upwards of 20 m of retreat in a single season (Table 1; Harper, 1990; Solomon, 2005; Radosavljevic, et al., 2016).

Ground ice in permafrost soils may be present in as pore ice, take the form of lenses, veins, and blocks, or comprise its own stratigraphic unit below the upper layer of sediment (Mackay, 1972; Murton, et al., 2004). While meltwater provides a medium of downlope transport for eroded soil constituents, the high ice-content of the ground material also means that only a fraction of the volume of eroded material contributes to the nearshore sediment budget (Kokelj, et al., 2009b; Dalimore, et al., 1996). Indeed, the Mackenzie River has been estimated to contribute approximately ten times more sediment annually to the Canadian Beaufort Sea than coastal erosion (Rachold, et al., 2000). The rate and variability of coastal erosion in the Canadian Beaufort Sea is affected by intrinsic factors, including ground material, ground-ice and permafrost occurrence, and coastal geomorphology, and by extrinsic variables, such as storm intensity and sea ice occurrence as controlled by atmospheric and hydrodynamic forcing (Solomon, 2005; Manson & Solomon 2007).

Increased retrogressive thaw slump (RTS; or “retrogressive thaw failure”; Couture, et al., 2015) activity since the 1950s has been observed on the western Beaufort Sea coast; these features are characterized by rapid local headwall retrogression due to exposed ground ice melt, creating bowl-shaped structures with steep headwalls of exposed ice-rich permafrost and thawed sediments in the slump floor (Ramage, et al., 2017; Lantuit & Pollard, 2008; Burn & Lewkowicz, 1990). The RTS morphology is in contrast to slumping coastal cliffs (Lantuit & Pollard 2005); although the thaw-related mobilization of ground material is similar in both instances, retreat in an RTS occurs rapidly from a point where ground ice is exposed, wheareas the coastal cliffs erode across long stretches at a relatively uniform rate, resulting in straighter cliff lines (Fig. 1).

Coastal retreat has implications from a terrain-loss perspective and for its potential chemical and atmospheric impact. The regression of coastlines, resulting in highly disturbed terrain or mobilization of ground material to the neashore, impinges on sensitive regions such as terrestrial ecosystems (Environment Canada, 2014), infrastructure and cultural sites of coastal communities (Mackay, 1986), and industrial infrastructure and waste storage sites (Kokelj & GeoNorth Ltd, 2002). Knowledge of erosive processes, trends and future threats is integral to predicting the future viability of the region as a subsistence-use region, and for any potential infrastructure or hydrocarbon development.

In addition to physical threat to terrestrial systems and land-use, coastal retreat of permafrost cliffs also act as a store of organic carbon, which may be liberated to the marine environment and to the atmosphere (Hugelius, et al., 2014). Organic carbon stored in the upper layers of sediment that is remobilized during erosion of ground material may be accumulated on the slope or shore, be incorporated into the nearshore sediment budget along with nitrogen and nutrient soil components, or can be released to the atmosphere by microbial mineralization (Cassidy, et al., 2016; Tanski, et al., 2017). While the amount of carbon dioxide released to the atmosphere is small in magnitude, it may be enough to offset the carbon sequestration of undisturbed tundra in the same region, resulting in a net positive contribution over the course of a growing season (Cassidy, et al., 2016).

Pullen Island, on the outer Mackenzie Delta, Northwest Territories (Fig. 2) has been observed intermittently for over seven decades, via aerial photography and ground surveys. The island's western cliffs are eroding via slumping and block failure, (Couture, et al., 2015), which is occuring over a relatively small area that is uniformly subject to extinsic environmental conditions. These long-term observations and the ability to differentiate erosion mechanisms affords an opportunity to assess specific geomorphic responses under recent changes in mean annual temperatures and storm intensities. We analyzed erosion processes resulting in cliff retreat, and sensitivities to summer air temperatures and storm events in order to investigate future trends under warming Arctic temperatures. Aerial imagery and ground survey data from 1947 to 2018 were used to determine cliff position and the dominant mechanism resulting in cliff retreat. Weather data from the Environment and Climate Change Canada station at Tuktoyaktuk were available from 1958 to 2018. Due to differences in measurement frequency, the study period used for regressions of weather and cliff retreat was 1967 to 2018.

The definition of "coastline" for this type of study is variable in the literature—broadly speaking, this can be any visually discernable line that separates the terrestrial and marine environments (Boak & Turner, 2005), and examples include the wet-dry line (e.g., Solomon, 2005), the slope base (e.g., Harper, 1978), the cliff edge (e.g., Solomon, et al., 1994), or the vegetation line (e.g. Cunliffe, et al., 2019). As such, in addition to cliff line retreat, this study also addresses two other possible measures of coastal change; shoreline and volumetric change. While in some areas the use of these different lines may yield similar measurements (such as very steep cliffs where the cliff edge and base of slope are inseparable in aerial imagery), these variable measures may have different implications depending on the slope morphology or the focus of the analysis (e.g., terrain loss versus sediment transfer, or marine impacts versus land use). To assess the differences in potential analytical results, "shoreline" retreat was assessed at the base of the slope in addition to the cliff retreat measurement (Fig. 1), as well as the change in volume of material based on Digital Surface Models (DSMs) generated by photogrammetry of imagery from 1992, 2016, 2017, and 2018.

2. Methods

2.1. Study area

Pullen Island, N.W.T., is part of the Mackenzie Delta on the Beaufort Sea shelf (Fig. 2). The island is comprised of tundra uplands and dynamic sand spits. The focus of this study is the west-facing ice-rich cliff; the eroding area includes near-vertical tundra cliffs failing through block collapse, slumping coastal cliffs, and RTS (Couture, et al., 2015). There are no in-depth reports on the state of cliff retreat on Pullen

Island, although it has been included in a multi-site publication of Mackenzie Delta stratigraphy (Murton, et al., 2004) and there are many reports of permafrost geomorphology and coastal processes in the Mackenzie Delta-Beaufort Sea region (e.g. Harper, et al., 1985; Baird, 1995; Taylor, et al., 1996; Solomon, 2005; Couture, et al., 2015).

As Pullen Island lies within the continuous permafrost zone, the ground below a certain depth remains frozen throughout the year. The island has a maximum elevation of 26 m at the top of the west-facing cliffs, and is marked by ice-wedge polygon networks. The upper layer of material that thaws seasonally is termed the active layer; this material is generally thought to be most susceptible to erosion in the summer months (Aré, et al., 2008). The thickness of the active layer is inherently linked to summer temperatures, which affect the depth to which the ground thaws.

Murton et al. (2004) identified two stratigraphic units on Pullen Island, accounting for the upper 16 m; sandy silt and massive ice. The sediment unit is approximately 12 m thick, and includes unlithified sandy silt, fine sand, and few pebbles to cobbles which are interpreted to have been brecciated subglacially at the margin of the Laurentide Ice Sheet, in addition to ice veins and blocks. The massive ice unit is at least 4 m thick, and is interpreted as buried basal ice (Murton, et al., 2004). The contact between the sediment unit and the underlying massive ice is an angular unconformity. Ground ice, as blocks and wedges, is visible in the cliff face. The west-facing cliff has been visually classified as having high ice content (>75%; Couture, et al., 2015).

2.2. Coastline digitization

Drone-based aerial imagery from 2016, 2017 and 2018 was processed using Pix4Dmapper photogrammetry software to produce georeferenced digital surface models (DSMs) and aerial imagery mosaics, georeferenced using ground control points measured during each survey. A DSM was similarly generated using aerial imagery from 1992 and elevation control points based current inland elevations.

A greater temporal extent has been achieved using historical aerial photographs, although at the cost of resolution and positional referencing quality (Table 2). The photographs, obtained from Natural Resources Canada archives, were scanned at 600 dpi and georeferenced in ArcMap. The control points used were primarily located at ice-wedge intersections, referenced to the 2016-2018 imagery.

Coastlines were identified based on slope morphology; the “cliff line” being the upper edge of the slope and the “shoreline” being the base. The lines were digitized by hand in ArcMap for each year with available imagery, and were drawn by a single user for consistency. GPS points from ground surveys of the cliff line in 2013-2015 were converted to lines in ArcMap and compiled with the digitized cliff lines in a single shapefile (Fig. 3). Cliff and shorelines from a total of 13 years spanning 1947-2018, were included in the final calculations (Table 2).

The positional error of each image was measured relative to the imagery for 2018. Because cliff retreat was calculated as the relative change in cliff line position, the error in geographic position is less important to the measurement than error in registration between images. Thus, the error was measured as the distance between the registered location of the same feature on the image in question and the 2018 imagery when the two where overlain in a GIS. Where identifiable on the imagery, 26 points were chosen for validation, which were not used as georeferencing points in the registration of the imagery. Imagery from 1985 had the maximum root mean square (RMS) positional error recorded (7.87 m relative to the 2018 imagery). The coarse resolution and low visual contrast of the 1985 imagery posed a particular challenge when locating control points for georeferencing as fewer landmarks (such as ice-wedge polygons) were visible.

For each year with imagery of sufficient resolution, sections of cliff were visually categorized as *clearly slumping*, *clearly block failure*, or *transitional*. Two areas were isolated for rate comparison; a section of cliff where the primary erosion mechanism is slumping, and a section dominated by block failure (Fig. 3). The cliff retreat rates were calculated for each period using transects that could be used to consistently compare both landward recession and form change through time.

2.3. Cliff retreat rate calculation

The Digital Shoreline Analysis System (DSAS; Theiler, et al., 2017), an extension for ArcMap, was used to calculate the rates of cliff line change. DSAS requires the user to input digitized cliff lines, over which transects are drawn from a user-defined baseline every 10 m. The system computes the distance between each point along a transect where it is intersected by a cliff line, and the positional difference between successive cliff lines can then be converted to mean annual retreat rates by dividing by the number of years between the two points. The mean rate was calculated for each pair of cliff-lines, and the mean annual values were used as the short-term rates. Three equal-interval periods (1947-1970, 1971-1994, and 1995-2018) were used for long-term rates calculations. Standard deviations have been calculated for each of the determined rates to represent the spatial variation occurring during each time period.

2.4. Volume change calculation

Volume change within the block failure and slump areas (Fig. 3) were calculated based on elevation differences of DSMs from 1992, 2016, 2017, and 2018. Positive and negative volume changes were calculated separately to differentiate areas of accretion or erosion of material, and then combined to find the net volume change. Values are reported as mean annual change in m^3 per 100 m of shoreline in the later year of the timestep (i.e., for 2017-2018, the length of the 2018 shoreline is used).

2.5. Air temperature and storms

Landfast ice (immobile sea ice that is fixed to the coast; Mahoney, 2018) has historically been present in the region between February and June in the Mackenzie Delta region, and there appears to be a trend of later onset of landfast ice formation by approximately 2.80 weeks per decade (mean formation and breakup for 1983-2009; Galley, et al., 2012). Considering the presence of pack ice, the traditional open water seasons have typically been between July and September (Solomon, 2005). The presence of sea ice up to the shore limits thermal erosion by wave action, so analysis was restricted to the open water season (Aré, et al., 2008; Wobus, et al., 2011). For this analysis, the open water season for inclusion of storm events was maintained as July to September, however it should be noted that some events outside of this period that could have impacted coastal retreat rates may have been excluded in the case of longer open water periods in a given year.

Wind and air temperature data from the Environment and Climate Change Canada weather station in Tuktoyaktuk, N.W.T., for the 1958-2018 open water seasons (July, August, and September) were processed using methods adapted from Atkinson (2005). Data were collected every 6 hours between 1958 and 1992, and hourly between 1993 and 2018. The dataset occasional gaps of ≤ 5 hours, approximately 30 gaps of 6 – 24 hours, and 8 gaps of > 24 hours. The missing times were excluded from the analysis, although we acknowledge that this may have resulted in missed or underestimated duration of storm events due to broken continuity of the record.

Storms were defined as events with wind speeds of at least 10 m s^{-1} sustained over at least 6 hours. These were filtered for events which would affect the actively eroding side of Pullen Island; storms with onshore wind directions between 270º and 15º from the north. "Synoptic duration" was calculated as the time between the first and last recorded wind speeds exceeding 10 m s^{-1} for each event. "Core duration" was calculated as the time during which wind speed was in the upper 50th percentile for each event. An example of the threshold wind speeds for a single event are shown in Fig. 4 to illustrate the definition of these storm duration values. The average synoptic and core durations and the mean air temperature have been calculated for every year on record. A 5-year moving average was calculated for each metric, and linear regressions (date against storm duration and date against temperature) were calculated using these averages to assess weather trends over the period of observation.

Satisfaction of the assumptions of linear regression was assessed for each of the dependent variables (cliff retreat across the study area, in the block failure area, and in the slump area) and independent variables (air temperature and core storm duration). Observations are independent from one another; the values used for each data point represent discrete periods of time. The independent variables are normally distributed. Although the the rates of cliff retreat in the slump area and over the entire study area are moderately left-skewed and the rates of retreat in the block failure area are severely right-skewed (skew coefficient of 1.3), the regressions do not exhibit heteroscedasticity when residuals are plotted against predicted values. As such, linear regression is considered acceptable for our purposes.

The mean cliff retreat rates for the entire study area and for each of the block failure and slump areas were regressed against mean air temperature and mean core storm duration. For this calculation, the mean weather metrics for the entire time step was compared to the annual rate of retreat. For example, the mean air temperature for all of 1967 to 1974 was used as the x-value to the mean retreat rate in the slump area for this period. Similar regressions were also calculated for mean air temperature and mean core duration against the mean retreat in the entire study area. For each regression, coefficients of determination (r^2) and probability values (p) were calculated, to comment on the significance of the observed relationships. Note that because weather data begin at 1958 and the next available imagery was from 1967, the first time interval for the long-term comparison only represents the step from the 1967 to 1974 imagery.

3. Results

The mean annual rate of cliff retreat, calculated over the entire study area, shows a three-phase increase: rising by 0.53 m a^{-1} decade^{-1} (1947 – 1985), through 1.8 m a^{-1} decade^{-1} (1985 – 2013) to an increase of 1.6 m a^{-2} (2013 – 2018; Fig. 5 A). The range of rates experienced across the study area also increased over time (Fig. 5 B). Certain areas, such as the west facing cliff section, maintained a more consistent rate of change throughout the study period, while others experienced more dramatic increases in cliff retreat rates (Fig. 6). The mean retreat rates were broken down into two categories based on failure mechanism, namely: “block failure” areas and “slump” failure areas (Fig. 5 C). While equal within one standard deviation to the mean cliff retreat rates for the corresponding time period, shoreline retreat rates show a more gradual trend over time: decreasing slightly by 0.15 m a^{-1}decade^{-1} (1947-1985), then rising by 1.2 m a^{-1} decade^{-1} (1985-2004), followed by 3.9 m a^{-1} decade^{-1} (2004-2018; Fig. 5 D). There was an overall increase in range of shoreline retreat rates across the study area (Fig. 5 E, however when divided by failure mechanism the area experiencing block failure remained more consistent through time, while the greatest change was in areas experiencing slumping (Fig. 5 F).

The mean annual volume change per 100 m of shoreline for each period (1992-2016, 2016-2017, 2017-2018), in each of the block failure and slump areas, is shown along with the mean rates of cliff and shoreline retreat (Fig. 8). Volume change over all time steps was greater in the slump area than the block failure area by an order of magnitude, however the same pattern is shown in both cases; the greatest change is seen over the 2016-2017 period.

The mean air temperature for July, August, and September recorded at Tuktoyaktuk has been calculated for each year between 1958 and 2018, in addition to a 5-year moving average. There is an increasing trend of 3°C per century (Fig. 9A), with annual variations within ±3°C of the trendline. Regressions of mean air temperature against rate of cliff retreat (Fig. 9B) reveal a positive, although statistically insignificant correlation across the entire study area ($r^2 = 0.34$; $p = 0.08$), in areas dominated by block failure ($r^2 = 0.08$; $p = 0.5$), and areas dominated by slumping ($r^2 = 0.41$; $p = 0.05$).

The mean annual synoptic and core duration of storms has been identified for the period between 1958 and 2018 (Fig. 9C). Regressions of mean core storm duration against rate of cliff retreat were calculated (Fig. 9D). Positive, but statistically insignificant relationships were found across the entire study area ($r^2 = 0.13$; $p = 0.3$) and in areas dominated by slumping ($r^2 = 0.34$; $p = 0.08$). There is a statistically significant relationship between core storm duration and cliff retreat in the block failure area ($r^2 = 0.84$; $p = 0.0002$).

4. Discussion

The observed rates of cliff and shoreline retreat on Pullen Island (3.4 ± 2.7 m a^{-1} and 2.3 ± 3.0 m a^{-1}, respectively) was within one standard deviation of the value of coastal retreat reported by Solomon (2005; see Table 1) for the outer Mackenzie Delta islands (1.5 ± 2.8 m a^{-1}) during comparable time periods (1974-2004 and 1972-2000). Over the entire period of observation (1947-2018), the northwest-facing sections of cliff experienced the most retreat, having lost as much as 330 m over this period and experiencing rates of cliff retreat up to 30 m a^{-1} in some areas. The mean annual rate over the whole study area has increased from 0 to 12 m a^{-1}. The increase in activity is not uniform across the entire cliff, however; the most change is seen around the RTS features, which experienced over 20 m a^{-1} headwall retreat in 2013-2018. Rates of retreat have also increased, although to a lesser degree, in both the non-retrogressive slump sections and block-failure sections (Fig. 6). Indeed, the long-term rates of cliff retreat in the block failure areas and areas of non-retrogressive slumping were primarily between 0 and 5 m a^{-1} between 1947 and 1993. In the following period, 1994-2018, the cliff sections were more variable with regard to rate of retreat; the standard deviation of retreat increased from 3.8 m a^{-1} to 6.5 m a^{-1}.

The correlations between retreat rate and both air temperature and core storm duration suggest that both have an influence on cliff retreat; this is in agreement with previous studies relating Arctic coastal erosion to these parameters, including Solomon, et al. (1994), who found that storm intensity was positively correlated with cliff retreat near Tuktoyaktuk and along the Yukon coast, and Günther, et al. (2015), who found that summer air temperature was positively correlated with cliff retreat on the Laptev Sea coast. Furthermore, we find that the impacts of air temperature and storm duration seem to have a greater or lesser effect depending on the dominant mechanism of erosion. It appears that warmer years see more cliff retreat, and more so in the slump areas than block failures. Similarly, years with longer duration of storms tend to experience more cliff retreat, and more so in the areas affected by block failures. This also suggests that, on a broad spatial scale, the decrease in homogeneity of retreat rate appears to be related to different magnitudes of response to environmental change, depending on the primary mechanism of cliff failure for a particular segment of coast.

4.1. Block failure responses

Block failure accounts for a small but annually increasing section of west-facing cliff. It occurs when the base of the cliff is undercut by waves and thermal erosion, and a whole block of material detaches from the cliff face due to lack of underlying support (Wobus, et al., 2011). The occurrence of block failure can be related primarily to the strength and frequency of storms (Baird 1995), which cause the surges that remove cliff-base sediment and induce thermal erosion at the cliff base. These erosion processes are limited to the open-water season, when sea ice has melted such that waves form and reach the cliff (Aré, et al., 2008; Wobus, et al., 2011). The two weather components assessed, summer air temperature and storm duration, have positive correlations with block failure. Warmer years are likely to have longer open-water seasons (Goegh-Guldberg, et al., 2018), and so have longer periods over which storms may generate waves to cause block failure.

Given the multi-year frequency and variable resolutions of imagery used, assessment of the relationship between weather and cliff retreat assumes that the mean trend effectively represents the mean annual trend. For example, the average number of storms over the time interval represented by the gap between images correlates with the mean retreat rate for that period. However, for much of the study period it cannot be established whether erosion during the survey-dependent time intervals occurred in the year with the most storms. Cliff change data at the annual resolution are only available for 2016-2018. Over this limited period, however, it was found that the three storms identified between 2016 and 2017 observations had longer core durations and faster wind speeds than the four storms between 2017 and 2018 observations, and that more cliff was lost in the block failure area in the 2016-2017 season. The long-term increasing trends in both summer air temperature and core storm duration suggest that there will be a continued increase in rate of cliff retreat in the block failure areas in the future.

4.2. Slump failure responses

The majority of the surveyed cliff area is eroded primarily through slumping failures, which in permafrost coasts is driven by ground ice melt. This releases previously-frozen sediment, removes support for overlying material, and entrains material as the meltwater runs downslope. Generally, the amount of melt depends on the net solar radiation that is received by the ground ice (Lewkowicz, 1986). The high latitude and well-constrained study area means that: (a) air temperature is an acceptable generic proxy for solar input, and (b) differences in melt are due to locally-defined slope angle and ice exposure, both of which impact net radiation. Theoretically, higher air temperatures would result in more melt, and thus more rapid headwall retreat; this is supported by the positive correlation between retreat rate and air temperature (Fig. 9 B).

There is notable heterogeneity of cliff retreat rates within areas of apparently similar erosion mechanisms, so lateral structural variations must also be considered. The most obvious distinction is between areas with RTS and those without. Along the northern-most cliffs, slumping occurs, but there is no development of discrete RTS features. In the central cliff section there are two large, pervasive RTS failures that can be tracked through the study period. The first is currently stable, but over the course of the study period has exhibited several periods of accelerated activity (some time prior to 1947, and for an unknown period between 1992 and 2013 that included 2004) and quiescence (between 1967 and 1985, and again around 2013). The second appears to have initiated around 2013 along the same slope as the former RTS, and retrogressed sufficiently to overtake the original headwall. This "polycyclic" RTS activity, where new slumps initiate on top of older, stabilized slumps, is observed elsewhere in the Beaufort Sea (Lantuit & Pollard, 2008). In the transitional and block failure areas small, recurring RTS have also been observed, which we will refer to as *perennial*, because they develop year after year on the same ice block but do not persist between melt seasons. This is in contrast to the large, *annual* RTS, which persist between melt seasons and thus can progress further from the headwall position attained the previous year.

The relationship between headwall retreat of an active RTS and meteorological data has been documented in regions near Pullen Island; there is a direct correlation between ablation of exposed ground ice and air temperature (Lewkowicz, 1986). Furthermore, there are several known factors which contribute to RTS initiation and maintenance of activity (or, inhibition of stabilization), including size of ice body, slope and ice face angles, and cliff height (Lewkowicz, 1986; 1987). Overall, the most important condition of continued RTS activity is that the ice remain exposed; if it becomes covered by sediment due to insufficient slope or melt to remove it, or if the ice body is exhausted, then activity will cease (Burn & Lewkowicz, 1990). Exposed ground ice appears to be primarily wedge ice formations, due to the lateral continuity between the ice and the network of polygon on the ground surface. Ice wedge polygon density on the surface appears fairly uniform over the whole slump area, so the lateral differences may cause some variation, but would likely even out over longer time scales.

Slope angle is generally steeper outside of RTS structures, however this is interpreted as a result of the slumps, and not their cause. Based on elevation models, it appears that the slope angle within an RTS reclines over time, while the slumping coastal cliffs maintain a more consistent slope angle (Fig. 10). Exposed ground ice has been observed throughout the study area, raising questions over why certain areas develop annual RTS structures, while other areas (with apparently similar structural characteristics and external forces) do not. There are two factors to consider that may play a large role in deciding the development of an RTS; cliff height, and adjacent cliff behavior.

Broadly speaking, ground materials that are mobilized downslope in an RTS system may come to rest on the headwall, accumulate on the slump floor, or enter the nearshore sediment budget. Lewkowicz (1987) attributed differences in sediment removal to headwall elevation; lower headwalls are more likely to have their ice covered by sediment, impeding ice ablation and halting thaw-related slumping. This is further supported by Ramage, et al. (2017), who found that coastal RTS activity on the Yukon coast was more likely to occur in areas with higher, steeper cliffs compared to lower or shallower slopes. In the context of our study area, the highest headwall elevations are found in the RTS area, with median elevation 23.5 m. This is followed by the non-RTS slump area, which has a median headwall elevation of 18 m. Finally, the block failure area has median headwall elevation of 6 m. A possible interpretation is that RTS structures developing in the block failure area tend to have their ice covered efficiently by sediment and subsequently cease activity. Perennial RTS are observed in the block failure area over successive years, but the adjacent cliff is retreating at such a rate that the characteristic bowl structure is removed before the end of the melt season and loses the positive feedbacks of increased surface area on ablation rate (Lacelle, et al., 2015). One determining parameter of the development of an annual RTS feature is sufficient activity to sustain a more rapid rate of retreat than the adjacent cliff sections. It is perhaps only necessary to maintain this localized elevated rate for a single melt season, such as to establish a bowl-shaped structure of sufficient size that will then begin the following melt season with higher retreat rates than the adjacent cliff. Due to the temporal resolution of the data, this cannot be confirmed for the identified annual RTS. Given the polycyclic nature of RTS, observed on Pullen Island and elsewhere in coastal (Lantuit & Pollard, 2008) and lakeside (Kokelj, et al., 2009) settings, one predictor of RTS activity is prior RTS activity in the region. Considering the history of the study area through the available imagery, it is unlikely that annual RTS structures such as those seen in the slump area will develop in the block failure area.

4.3 Alternative coastal change measurements: Shoreline retreat and volume change

Measurements of mean annual retreat of the shoreline (defined here as the base of the slope) yielded similar trends to cliff retreat, being equal within one standard deviation and following the increase in rate over time, although to a lesser degree until the latest period of acceleration (Fig. 5). This would suggest that using either the shore or the cliff line give an adequate broad sense of coastal change through time, but that at the annual resolution are somewhat disconnected from one another, and from measures of volumetric change.

A preliminary statement about the link between shoreline, cliff line, and volumetric changes can be made based on the four DSMs included in this analysis (1992, 2016, 2017, 2018). When the volumetric change over the block failure and slump areas were calculated from elevation difference between consecutive DSMs, it appears that volume is more directly related to retreat in the block failure area than in the slump area. In the area dominated by block failure, years of greater cliff and shoreline retreat also have greater volume of material lost. In the area affected by slumping, the pattern of volume loss tracks more closely with retreat of the cliff line, while there appears to be a disconnect between volume loss and shoreline retreat; the greatest mean annual volume change of the three periods occurred in 2016-2017, while the greatest shoreline retreat occurred in 2017-2018 (Fig. 8).

One potential explanation for the disconnect between shoreline, cliff line, and volume changes are the pathways for eroded material depending on the dominant erosive mechanism. Obu, et al. (2016), observed that within their study area on Herschel Island, Yukon, volumetric change was more laterally uniform than planimetric measurements of coastal change, and that some of the short term variability in coastal retreat was related to lag between detachment of material from the slope and removal from the shore. In areas being eroded by block failure, material is detached simultaneously from the cliff edge and observable slope base, then removed to the nearshore environment over a period of a couple weeks (Barnhart, et al., 2014). It follows, therefore, that planimetric measures of coastal change and loss of material would follow similar trends.

Where the cliff is being eroded by slumping, material is not removed simultaneously from the cliff edge and slope base; sediments may be deposited on the slope, in the base of an RTS, or at the base of the slope, before being removed to the nearshore. Indeed, some net accumulation of sediments is observed within the active RTS in 2016-2017 and 2017-2018 (Fig. 7 B & C; up to 3 m surface elevation increase). Discrepancies between the amount of material removed from the cliff and from the shore may be the result of redeposition prior to reaching the shore (Obu, et al., 2016), volume change due to ice melt (Couture, et al., 2018), or due to short-term inconsistencies related to the processes driving sediment movement on the cliff edge (i.e. gravity-driven mobilization) and the slope base (i.e. wave action).

The connections drawn here between volume change and cliff and shoreline retreat on Pullen Island are preliminary due to the inclusion of only three time periods in the analysis. There is some suggestion in the literature that over sub-annual period there would be more disconnect between cliff and shoreline change, which tend to equilibrate over the course of one or more seasons (Barnhart, et al., 2014). The appropriate metric of coastal change likely depends on the application of this value. Net change in volume may be the most representative, if not the most intuitive metric to apply practically. Adjusting volumetric measurements to account for ice content, thus reporting the change in sediment volume, has been applied to studies of mobilization of carbon, nitrogen, and other soil constituents and impacts on the marine environment (e.g., Couture, et al., 2018; Ramage, et al., 2018). Changes to shoreline is a commonly used value, and similarly relates to the nearshore sediment budget (e.g., Harper, 1978; Solomon, 2005). However, for applications regarding terrain loss, impacting terrestrial ecosystems and human land-use and infrastructure, cliff retreat appears to be the most intuitive measurement to report, especially considering the increaing RTS activity across the Canadian Beaufort Sea Coast, and the potential for discrepancy between cliff and shoreline retreat over short periods of time.

4.4 Other explanators of coastal retreat

The stratigraphy of Pullen Island is one of the most important factors controlling how rapidly the cliffs are eroding, and their response to other environmental drivers. The ice fraction of eroded material melts and does not become redeposited (Harper, et al. 1985), which contributes to the extreme rates of cliff retreat experienced in this area compared to non-permafrost coasts. Limiting sediment as talus prolongs ice exposure and increases local relief (Kokelj, et al., 2015; Aré, 1988), and leaves the cliff base exposed to thermal and mechanical abrasion (Baird, 1995; Aré, 1988).

Slope aspect may also impact cliff retreat as it relates to insolation, which provides the energy to thaw the active layer and sustain RTS activity (Lewkowicz, 1986). Variations in aspect within the study area can result in local differences in net radiation (Lewkowicz, 1986; 1987). The eroding coasts on Pullen Island range from north-facing in the north of the study area, to west-facing in the south of the study area. Being in the northern hemisphere, the more west-facing slope will receive more direct solar radiation than the north-facing region. However, it is noted that the diffuse sunlight at this latitude and extended polar day mean that the impact is likely not very large compared to other factors which drive coastal retreat (Wobus, et al., 2011; Aré, 1988). Nonetheless, variation in slope aspect may help to explain, at least in part, the lateral differences in retreat rate of the slumping coastal cliffs in the later years of observation (Fig. 6).

The relationship between failure, transport, and deposition in the nearshore environment is somewhat iterative. The amount of failure determines the volume available to be deposited; this volume decreases when the ice fraction melts. The volume deposited at the base of the slope in turn affects the amount of erosion; where there is less sediment available to protect the base of the slope, more rapid removal of material should occur. The balance is maintained by ice content and slope, which influence effective transport; however, these variables are also dependent on the mechanisms of failure and deposition. Changes to one or more of these factors, such as increased air temperatures resulting in more melt or longer open-water seasons and hence the susceptibility to wave action, resulting in a change to the other processes in the cycle. While the finer nuances of these relationships are beyond the scope of this paper, the movement of material and the characteristics (ice content, cliff height, air temperature, etc.) of the local environment in which it takes place are essential and interdependent controls on the rate of retreat of ice rich permafrost cliffs.

5. Conclusions

The rate and variability of retreat across the ice-rich cliffs of Pullen Island have increased over the 71 years of observation; the island has gone from a mean annual retreat of < 1 m with standard deviation of 2.1 during the 1940s to 1980s, to 12 m a^{-1} retreat with standard deviation of 6.3 in the final five years of the study. The acceleration in retreat is interpreted primarily as response to increasing air temperatures causing increased ground ice melt. The magnitude of response to air temperature change depends on the dominant erosive mechanism for a particular section of cliff; the slump-dominated cliffs, specifically around the RTS features, accelerated faster than the block failure-dominated sections. The decreasing uniformity of cliff retreat is expected to continue in response to current air temperature trends.

Between 1947 and 2018, Pullen Island experienced cliff line retreat of up to 330 m in some areas, of which up to 50 m retreat occurred between 2013 and 2018. In 2018, the width of the island was approximately 550 m behind the more slowly eroding areas, and between 250 m and 500 m behind the more rapidly eroding areas. If the current retreat rate of 12 m a^{-1} is sustained, Pullen Island will cease to exist in its currently recognizable form by the year 2060. Considering the acceleration of retreat that is experienced, however, this may come ten or fifteen years sooner, given the mean long-term acceleration of 0.2 m a^{-1} since 1947, or that of 1.6 m a^{-1} seen between 2013 and 2018.

Both shoreline and cliff line reatreat rates are used as measures of coastal change thoughout the literature, However, the short-term disconnect between the two metrics may be exacerbated by increased slump activity in the Mackenzie Delta region (Couture, et al., 2015; Barnhart, et al., 2014). The respective implacations for marine and terrestrial impacts of shoreline or cliff line change rates suggests that care should be taken to report the appropriate values depending on their intended application. Where issues of terrain loss are concerned, cliff line retreat appears to be the more intuitive and useful metric of coastal change.

As noted, these conclusions are based on trends of multi-year averages. Future work in this area, with a greater frequency of measurements allowing for annual resolution, will be required to better understand the strength of the relationship between the mechanisms driving cliff retreat and environmental factors. Nevertheless, it is apparent that mechanism-specific magnitudes of response to environmental change contributes to the dynamic complexities of permafrost cliff systems.

Acknowledgement

Funding and support for this project was provided by Natural Resources Canada through the Climate Change Geoscience Program and Polar Continental Shelf Project (PCSP). Additional funding was provided by the Inuvialuit Regional Corporation (IRC) and Crown-Indigenous Relations and Northern Affairs Canada (CIRNAC) through the Beaufort Sea Regional Strategic Environment and Research Assessment (BRSEA). In addition, this work was made possible through the Natural Environment and Research Council (NERC) sponsored UK-Canada Arctic bursary program. We are grateful to the field crews, in particular Paul Fraser, Angus Robertson, Roger Macleod from NRCan and Andrew Clark from the University of Calgary for acquiring the UAV data used in this study. We would also like to acknowledge the Aurora Research Institute (ARI), the Inuvialuit Game Council, and the communities and Hunters and Trappers Committees of Inuvik and Tuktoyaktuk for their continued support.

References

Aré, F. E., 1988. Thermal abrasion of sea coasts (part I). Polar Geography and Geology, 12(1), p. 1.

Aré, F., Reimnitz, E., Grigoriev, M., Hubberten, H.-W., & Rachold, V., 2008. The influence of cryogenic processes on the erosional Arctic shoreface. Journal of Coastal Research, 24(1), pp. 110-121.

Atkinson, D. E., 2005. Observed storminess patterns and trends in the circum-Arctic coastal regime. Geo-Marine Letters, 25(2), pp. 98-109.

Baird, W. F., 1995. Thermal-mechanical model for erosion processes on Arctic coasts, s.l.: s.n.

Barnhart, K. R., Anderson, R. S., Overeem, I., Wobus, C., Clow, G. D., Urban, F. E., 2014. Modeling erosion of ice-rich permafrost bluffs along the Alaskan Beaufort Sea coast. Journal of Geophysical Research: Earth Surface, 119, doi: 10.1002/2013JF002845

Boak, E. H., Turner, I. L., 2005. Shoreline definition and detection: A review. Journal of Coastal Research. 214, pp. 688-703. doi: 10.2112/03-0071.1

Burn, C. R. & Lewkowicz, A. G., 1990. Retrogressive thaw slumps. The Canadian Geographer, Volume 34, pp. 273-276.

Cassidy, A. E., Christen, A., Henry, G. H. R., 2016. The effect of a permafrost disturbance on growing-season carbon dioxide fluxes in a high Arctic tundra ecosystem. Journal of Geophysical Research: Biogeosciences, 13, pp. 2291-230. doi: 10.5194/bg-13-2291-2016

Cunliffe, A. M., Tanski, G., Radosavljevic, B., Palmer, W. F., Sachs, T., Lantuit, H., Kerby, J. T., Myers-Smith, I. H., 2019. Rapid retreat of permafrost coastline observed with aerial drone photogrammetry. The Cryosphere, 13, pp. 1513-1528. doi: 10.5194/tc-13-1513-2019

Couture, N. J., Forbes, D. L., Fraser, P. R., Frobel, D., Jenner, K. A., Manson, G. K., Solomon, S. M., Szlavko, B., Taylor, R. B., 2015. A coastal information system for the southeastern Beaufort Sea, Yukon and Northwest Territories. Geological Survey of Canada Open File 7778.

Couture, N. J., Irrgang, A., Pollard, W., Lantuit, H., Fritz, M., 2018. Coastal erosion of permafrost soils along the Yukon Coastal Plain and fluxes of organic carbon to the Canadian Beaufort Sea. Journal of Geophysical Research: Biogeosciences, 123(2), pp. 406-422. doi: 10.1002/2017JG004166

Dallimore, S. R., Wolfe, S. A., Solomon, S. M., 1996. Influence of ground ice and permafrost on coastal evolution, Richards Island, Beaufort Sea coast, N.W.T. Canadian Jounral of Earth Sciences, 33, pp.664-675.

Environment Canada, 2014. Coastal and nearshore bird usage of the Canadian Beaufort Sea. Data prepared by the Canadian Wildlife Service (CWS) and Upon-LGL Limited.

Goegh-Guldberg, O. D., Jacob, D., Taylor, M., Bindi, M., Brown, S., Camilloni, I., Diedhiou, A., Djalante, R., Ebi, K. L., Engelbrecht, F., Guiot, J., Hijioka, Y., Mehrotra, S., Payne, A., Seneviratne, S. I., Thomas, A., Warren, R., Zhou, G. 2018. Impacts of 1.5^{o}C global warming on natural and human systems. In: V. Masson-Delmotte, V., Zhai, P., Portner, H.-O., Roberts, D., Skea, J., Shukla, R. P., Pirani, A., Moufouma-Okia, W., Pean, C., Pidock, R., Connors, S., Matthews, J. B. R., Chen, Y., Zhou, X., Gomis, M. I., Lonnoy, E., Maycock, T., Tignor, M., Waterfield, T. eds. Global warming of 1.5^{o}C. An IPCC Special Report on the impacts of global warming of 1.5^{o}C above pre-industrial levels and related global greenhouse gas emission pathways, in the context of strengthening the global response to the threat of climate change, sustainable development, and efforts to eradicate poverty.

Günther, F., Overduin, P. P., Yakshina, I. A., Opel, T., Baranskaya, A. V., Grigoriev, M. N., 2015. Observing Muostakh disappear: permafrost thaw subsidence and erosion of a ground-ice-rich island in reponse to arctic summer warming and sea ice reduction. The Cryosphere, 9(1), pp. 151-178. doi: 10.5194/tc-9-151-2015

Harper, J. R., 1978. Coastal erosion rates along the Chukchi Sea coast near Barrow, Alaska. Arctic, 31(4), pp. 428-433.

Harper, J. R., 1990. Morphology of the Canadian Beaufort Sea Coast. In: P. R. Hill, ed. The Beaufort Sea coastal zone. Marine Geology, pp. 75-91.

Harper, J. R., Reimer, P. D., Collins, A. D., 1985. Canadian Beaufort Sea: Physical shore-zone analysis. Geological Survey of Canada Open File 1689.

Hugelius, G., Strauss, J., Zubrzycki, S., Harden, J. W., Schuur, E. A. G., Ping, C.-L., Grosse, G., Michaelson, G. J., Koven, C. D., O'Donnell, J. A., Elberling, B., Mishra, U., Camill, P., Yu, Z., Palmtag, J., Kuhry, J. A. 2014. Estimated stocks of circumpolar permafrost carbon with quantified uncertainty ranges and identified data gaps. Journal of Geophysical Research: Biogeosciences, 11, pp. 6573-6593. doi: 10.5194/bg-11-6573-2014

Kokelj, S. V., & GeoNorth Ltd., 2002. Drilling mud sumps in the Mackenzie Delta Region: Construction, abandonment and past performance. Report to the Department of Indian Affairs and Northern Development, Northwest Territories Region. 16 p.

Kokelj, S. V., Lantz, T.C., Kanigan, J., Smith, S.L., Coutts, R. 2009a. Origin and polycyclic behaviour of tundra thaw slumps, Mackenzie Delta region, Northwest Territories, Canada. Permafrost and Periglacial Processes, 20(2), pp. 173-184.

Kokelj, S. V., Zaidlik, B., Thompson, M. S. 2009b. The impacts of thawing permafrost on the chmistry of lakes across the subarctic boreal-tundra transition, Mackenzie Delta region, Canada. Permafrost and Periglacial Processes, 20, pp. 185-199. doi: 10.1002/ppp.641

Kokelj, S. V., Tunnicliffe, J., Lacelle, D., Lantz, T.C., Chin, K.S., Fraser, R. 2015. Increased precipitation drives mega slump development and destabilization of ice-rich permafrost terrain, northwest Canada. Global and Planetary Change, Volume 129, pp. 56-68.

Lacelle, D., Brooker, A., Fraser, R. H., Kokelj, S. V., 2015. Distribution and growth of thaw slumps in the Richardson Mountains-Peel Plateau region, northwestern Canada. Geomorphology, Volume 235, pp. 40-51.

Lantuit, H. & Pollard, W. H., 2005. Temporal stereogrammetric analysis of retrogressive thaw slumps on Herschel Island, Yukon Territory. Natural Hazards and Earth Systems Sciences, 5, pp. 413-423.

Lantuit, H. & Pollard, W. H., 2008. Fifty years of coastal erosion and retrogressive thaw slump activity on Herschel Island, Southern Beaufort Sea, Yukon Territory, Canada. Geomorphology, 95(1), pp. 84-102.

Lewkowicz, A. G., 1986. Rate of short-term ablation of exposed ground ice, Banks Island, Northwest Territories, Canada. Journal of Glaciology, 32(112), pp. 511-519.

Lewkowicz, A. G., 1987. Headwall retreat of ground-ice slumps, Banks Island, Northwest Territories. Canadian Journal of Earth Science, Volume 24, pp. 1077-1087.

Mackay, J. R., 1986. Fifty years of coastal retreat west of Tuktoyaktuk, District of Mackenzie. Current Research, Part A, Geological Survey of Canada, Paper 86-1A, pp. 727-735. doi: 10.4095/120445

Mackay, J. R., 1972. The world of underground ice. Annals of the Association of American Geographers, 62(1), pp. 1-22. doi: 10.1111/j.1467-8306.1972.tb00839.x

Manson, G. K. & Solomon, S. M., 2007. Past and future forcing of Beaufort Sea coastal change. Atmosphere-Ocean, 45(2), pp. 107-122.

Murton, J. B., Waller, R. I., Hart, J. K., Whiteman, C. A., Pollard, W. H., Clark, I. D. 2004. Stratigraphy and glaciotectonic structures of permafrost deformed beneath the northwest margin of the Laurentide Ice Sheet, Tuktoyaktuk Coastlands, Canada. Journal of Glaciology, 50(170), pp. 399-412.

Obu, J., Lantuit, H., Fritz, M., Pollard, W. H., Sachs, T., Günther, F., 2016. Relation between planimetric and volumetric measurements of permafrost coast erosion: a case study from Herschel Island, western Canadian Arctic. Polar Research, 35(1), 30313, doi: 10.3402/polar.v35.30313

Rachold, V., Grigoriev, M. N., Aré, F. E., Solomon, S., Reimnitz, E., Kassens, H., Antonow, M, 2000. Coastal erosion vs riverine sediment discharge in the Arctic Shelf seas. International Journal of Earth Sciences, 89(3), pp. 450-460.

Radosavljevic, B., Lantuit, H., Pollard, W., Overduin, P., Couture, N., Sachs, T., Helm, V., Fritz, M., 2016. Erosion and flooding - threats to coastal infrastructure in the Arctic: A case study from Herschel Island, Yukon Territory, Canada. Estuaries and Coasts, 39(4), pp. 900-915.

Ramage, J. L., Irrgang, A. M., Herzchuh, U., Morgerstern, A., Couture, N., Lantuit, H. 2017. Terrain controls on the occurrence of coastal retrogressive thaw slumps along the Yukon Coast, Canada. Journal of Geophysical Research: Earth Surface, 122, pp. 1619-1634. doi: 10.1002/2017JF004231

Ramage, J. L., Irrgang, A. M., Morgerstern, A., Couture, N., Lantuit, H., 2018. Increasing coastal slump activity impacts the release of sediment and organic carbon into the Arctic Ocean. Journal of Geophysical Research: Biogeosciences, 15, pp. 1483-1495. doi: 10.5194/bg-15-1483-2018

Solomon, S. M., 2005. Spatial and temporal variability of shoreline change in the Beaufort-Mackenzie region, Northwest Territories, Canada. Geo-Marine Letters, Volume 25, pp. 127-137.

Solomon, S. M., Forbes, D. L., Kierstead, B., 1994. Coastal impacts of climate change: Beaufort Sea erosion study. Geological Sruvey of Canada, Open File 2890, 85 p. doi: 10.4095/194148

Statistics Canada, 2016a. 2016 Census – Boundary files: Lakes and rivers (polygons), cartographic boundary file [shapefile]. Statistics Canada Catalogue.

Statistics Canada, 2016b. 2016 Census – Boundary files: Provinces/territories, water file [shapefile]. Statistics Canada Catalogue.

Tanski, G., Lantuit, H., Ruttor, S., Knoblauch, C., Radosavljevic, B., Strauss, J., Wolter, J., Irrgang, A. M., Ramage, J., Fritz, M., 2017. Transformation of terrestrial organic matter along thermokarst-affected permafrost coasts in the Arctic. Science of the Total Environment, 581, pp. 434-447. doi: 10.1016/j.scitotenv.2016.12.152

Taylor, A. E., Dallimore, S. R., Judge, A. S., 1996. Late Quaternary history of the Mackenzie-Beaufort region, Arctic Canada, from modelling of permafrost temperatures. 2. The Mackenzie Delta - Tuktoyaktuk Coastlands. Canadian Journal of Earth Science, 33(1), pp. 62-71.

Thieler, E. R., Himmelstoss, E. A., Zichichi, J. L., Ergul, A., 2017. The Digital Shoreline Analysis System (DSAS) Version 4.0 - An ArcGIS extension for calculating shoreline change. U.S. Geological Survey Open-File Report 2008-1278.

Wobus, C., Anderson, R., Overeem, I., Matell, N., Clow, G., Urban, F. 2011. Thermal erosion of a permafrost coastline: Improving process based models using time-lapse photography. Arctic, Antarctic, and Alpine Research, 43(3), pp. 474-484.

Tables

Table 1. Summary of annual coastal retreat rates for the Canadian Beaufort Sea-Mackenzie Delta region over the preiod of 1972-2000 reported by Solomon (2005).

Region	Mean (m a^{-1})	Standard deviation (m a^{-1})
Outer Mackenzie Delta	1.77	1.82
East Richards Island	0.40	0.62
Outer Mackenzie Delta Islands	1.51	2.79
West Richards Island	0.46	0.79
Tuktoyaktuk Peninsula	0.75	1.28

Table 2. Resolution and root mean square (RMS) positional error of aerial imagery relative to 2018 imagery.

Year	Pixel size (m)	RMS positional error (m)
1947	1.35	6.09
1950	1.29	5.14
1967	1.29	4.09
1974	1.88	4.55
1985	4.67	7.87
1992	0.25	2.45
2004	0.5	1.76
2016	0.025	0.48
2017	0.025	0.29
2018	0.025	-

Figures

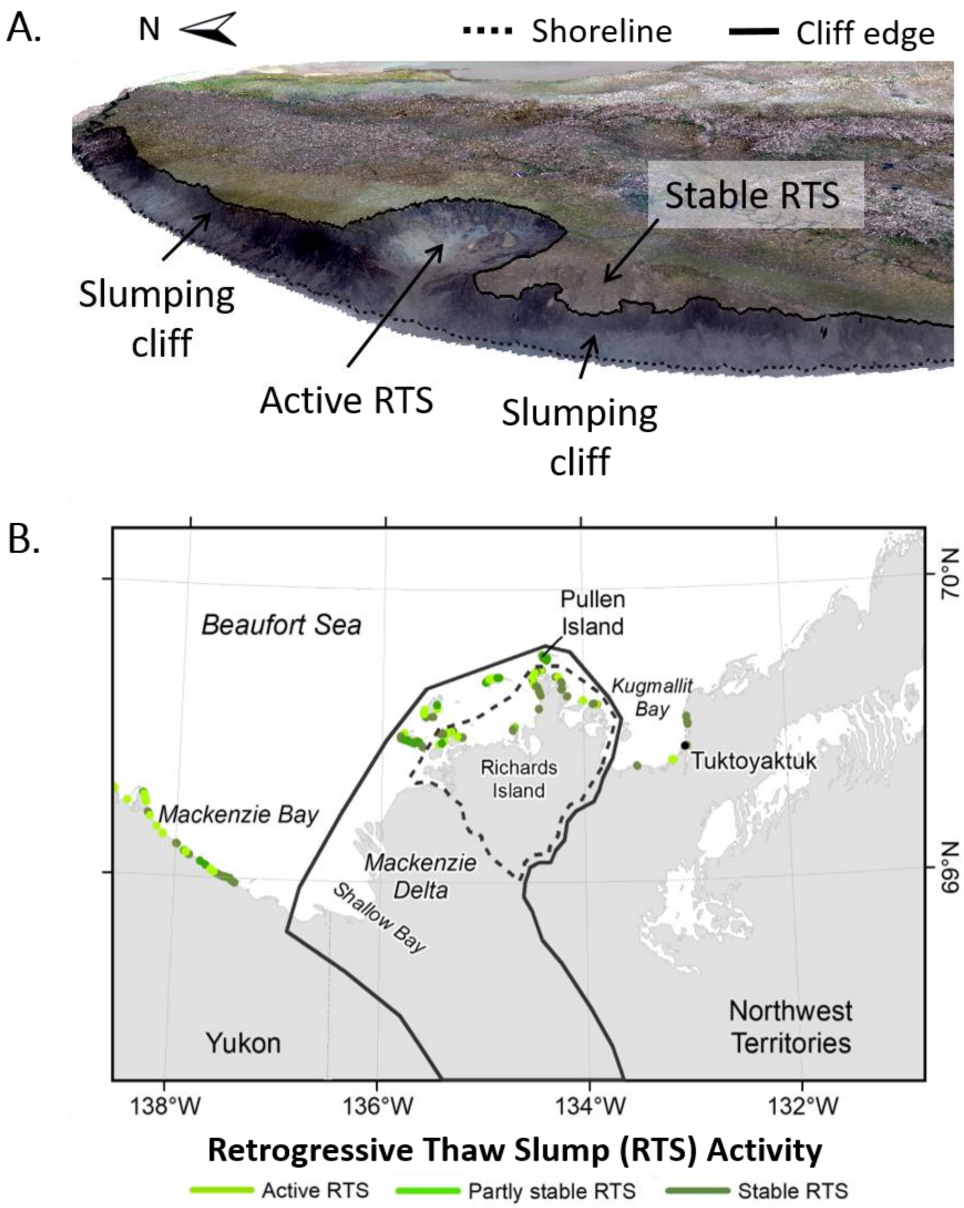

Fig. 1. (A) Oblique view of an active retrogressive thaw slump (RTS), stable RTS, and slumping coastal cliffs on Pullen Island, Northwest Territories (imagery courtesy of the Geological Survey of Canada, 2018). (B) Active, partially stable, and stable RTS occurrences in the Mackenzie Delta region of the Canadian Beaufort Sea coast (Couture, et al., 2015).

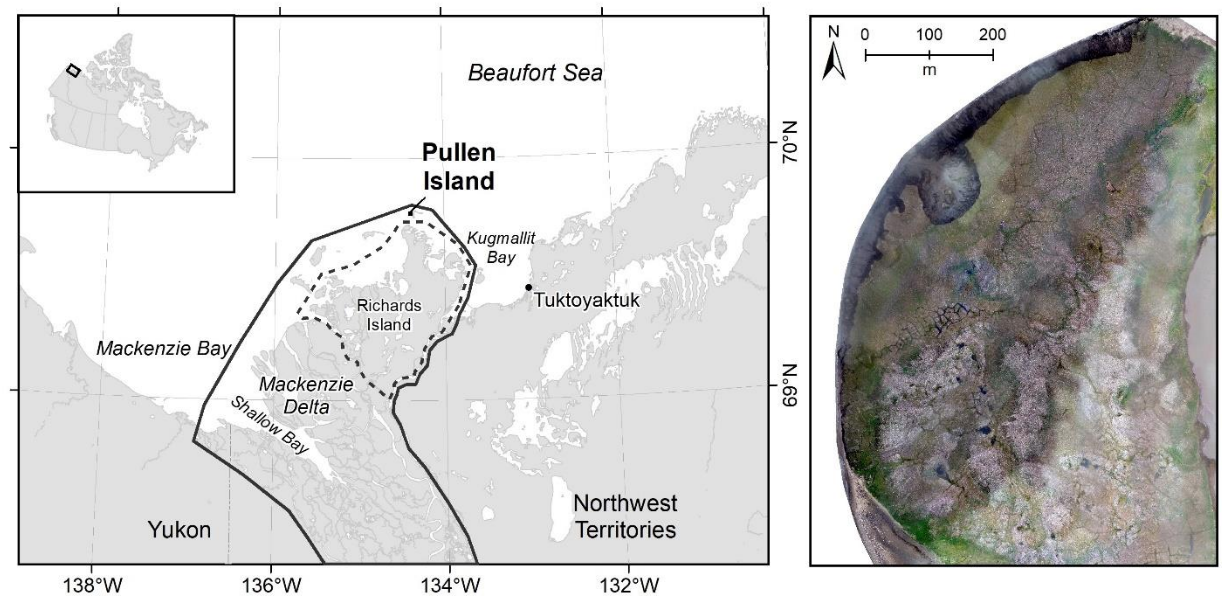

Fig. 2. Location of Pullen Island on the Mackenzie Delta, N.W.T. Aerial imagery courtesy of the Geological Survey of Canada (2018) and base imagery from Statistics Canada (2016a; 2016b).

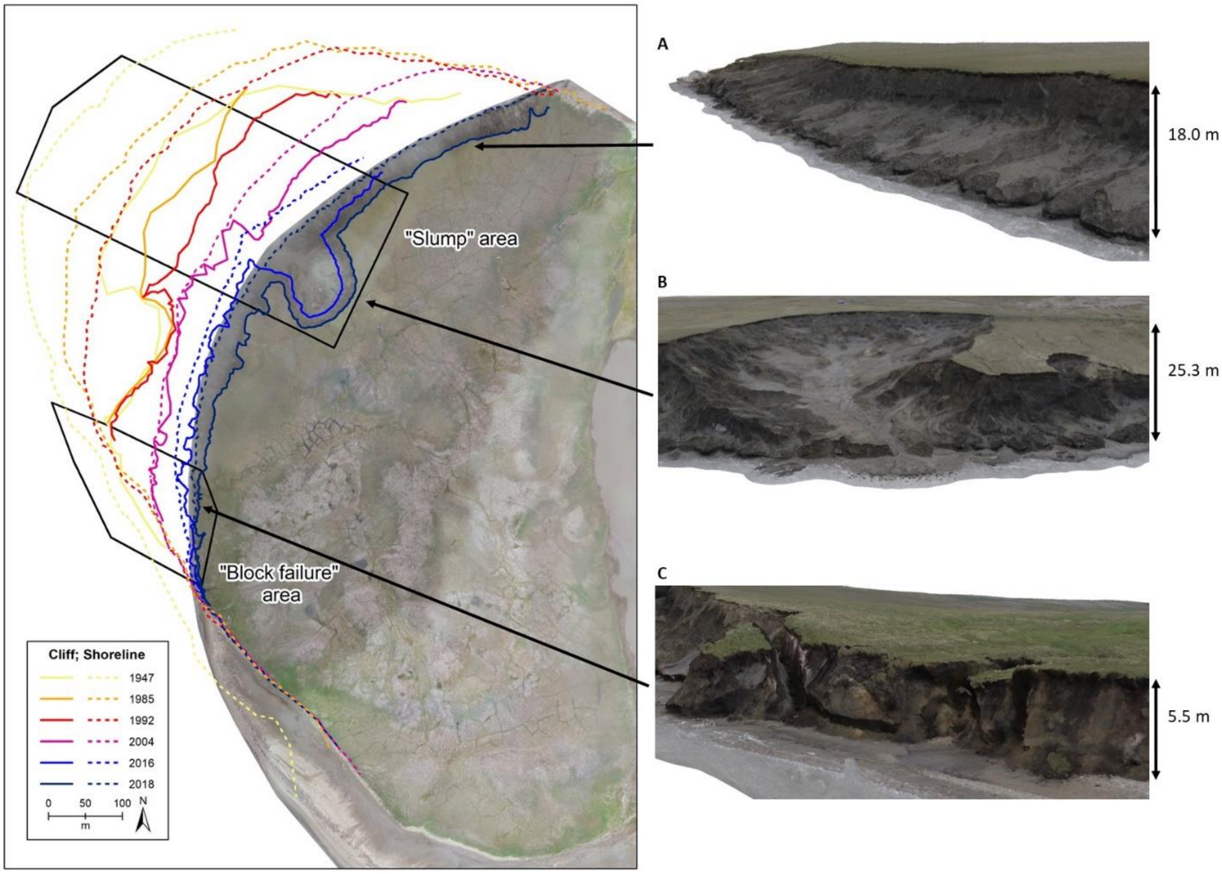

Fig. 3. Location of cliff and shorelines on Pullen Island, N.W.T., 1947-2018. Lines from 1950, 1967, 1974, 2013, 2014, 2015, 2017 excluded for simplicity. Outlined are areas designated as dominated by slump or by block failure for erosion rate comparison. Oblique images show sections of (A) slumping coastal cliffs, (B) retrogressive thaw slumping, and (C) block failure, as seen in the 2018 3D model. Imagery courtesy of the Geological Survey of Canada (2018)

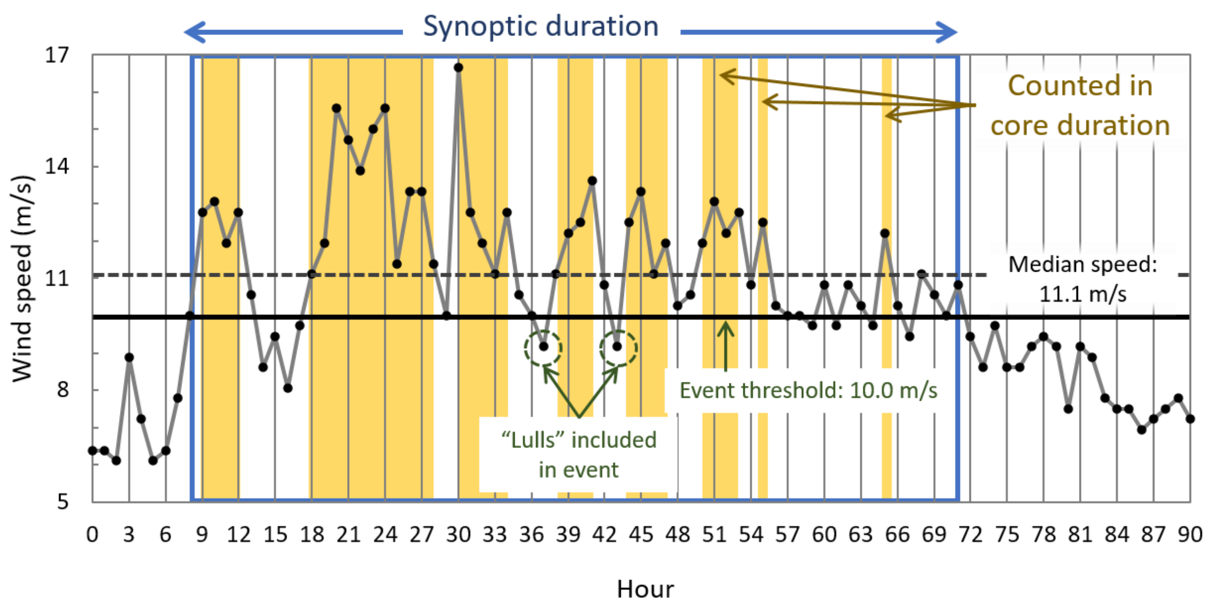

Fig. 4. An example storm event (July 18-21, 2016; Environment and Climate Change Canada, 2016) to illustrate threshold wind speeds in definition of synoptic and core storm duration, per Atkinson (2005). The entire storm event is contained within the blue box, the length being equal to the synoptic duration. Periods during which the wind speed is equal to or greater than the median speed for the event, highlighted in yellow, are counted into the core duration.

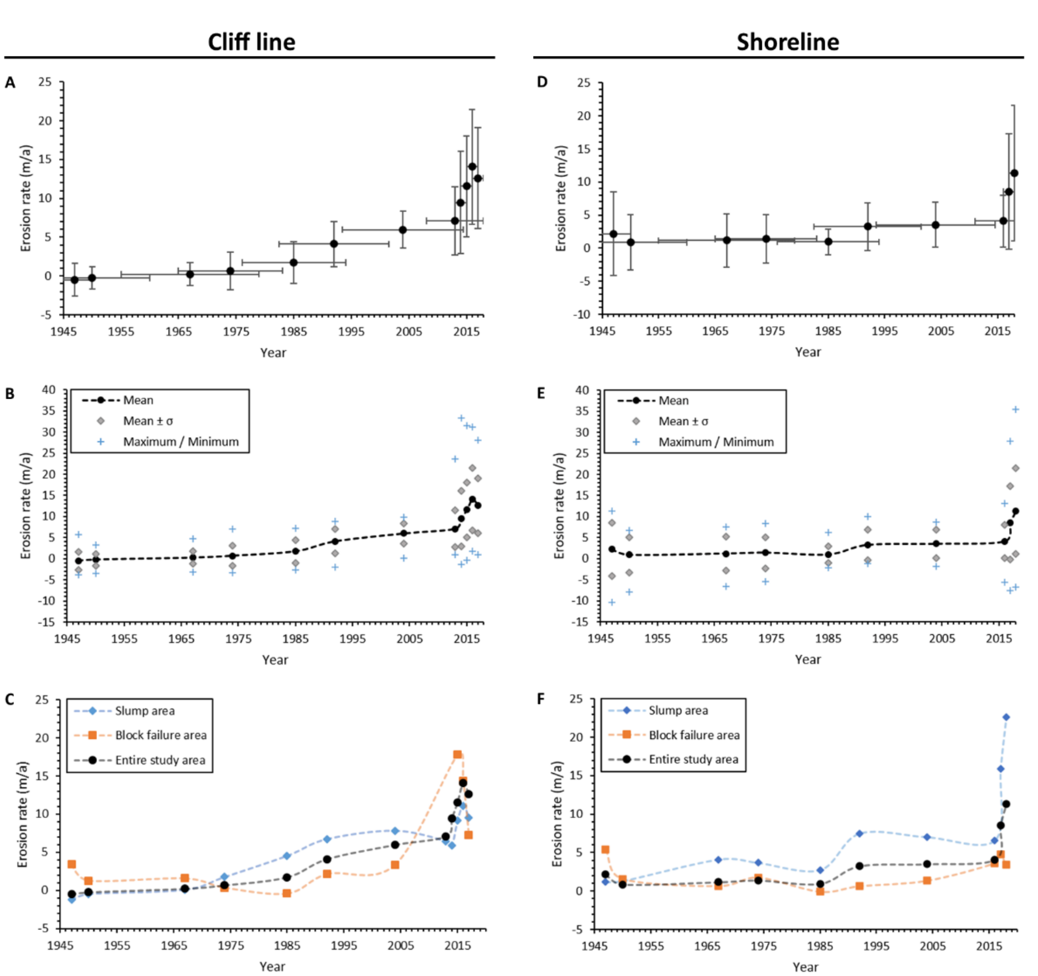

Fig. 5. Mean annual erosion rates on Pullen Island, N.W.T., 1947-2018. (A) Mean cliff line erosion rate of the entire study area. Horizontal error bars are proportional to the number of years over which the measurements are averaged, and vertical error bars are proportional to the positional error of the source data. (B) Mean, maximum, minimum, and standard deviation of the annual cliff erosion rates for the entire study area. (C) Mean rate of cliff retreat in the slumping and block failure areas. (D) Mean shoreline erosion rate of the entire study area. Horizontal error bars are proportional to the number of years over which the measurements are averaged, and vertical error bars are proportional to the positional error of the source data. (E) Mean, maximum, minimum, and standard deviation of the annual shoreline erosion rates for the entire study area. (F) Mean rate of shoreline retreat in the slumping and block failure areas.

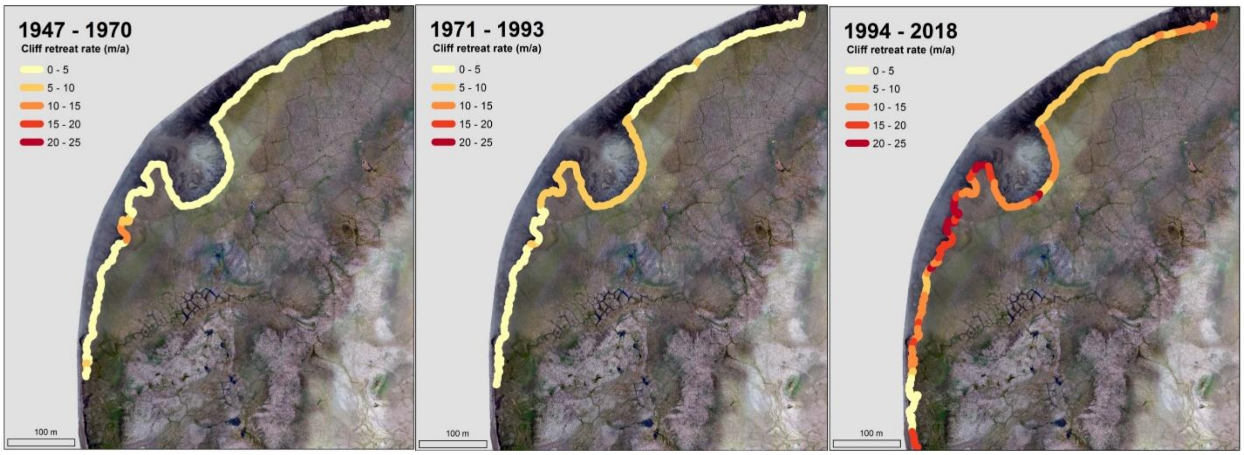

Fig. 6. Mean rate of annual cliff retreat through time. Focusing on the northwest area of Pullen Island, mean rates for each time period (1947-1970, 1971-1993, 1994-2018) are displayed on an equal interval scale of 5 m a^{-1}. Imagery courtesy of the Geological Survey of Canada (2018)

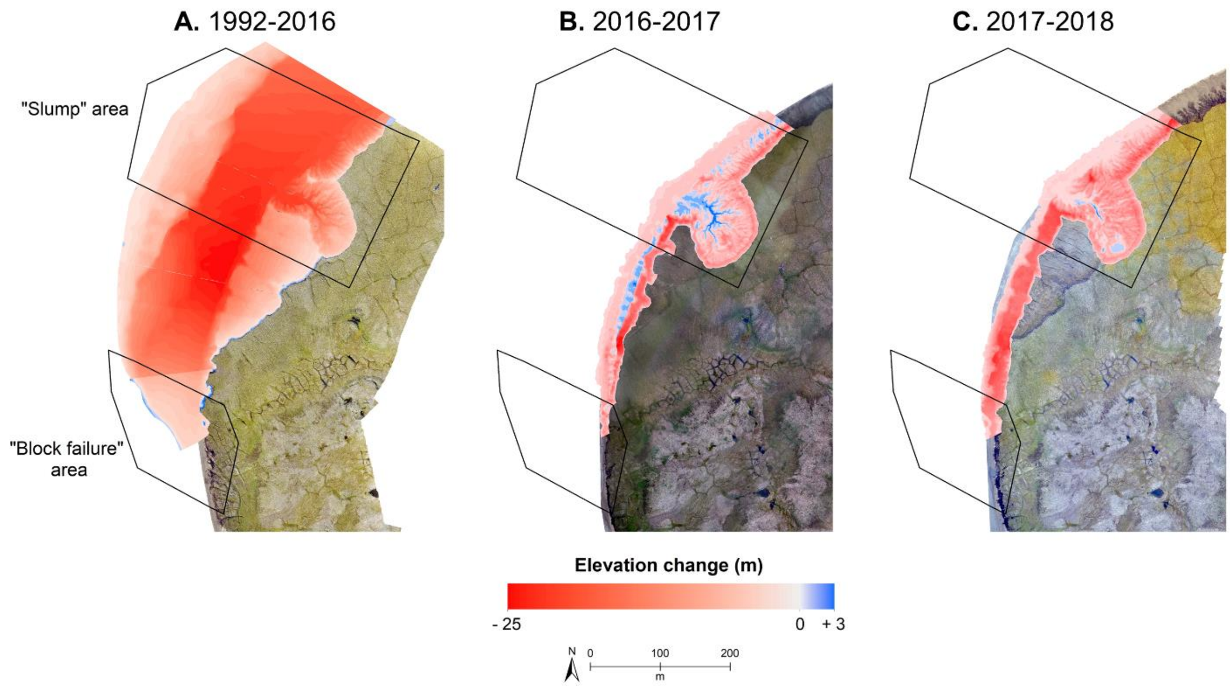

Fig. 7. Elevation difference between Digital Surface Models over (A) 1992-2016, shown over imagery from 2016; (B) 2016-2017, shown over imagery from 2017; and (C) 2017-2018, shown over imagery from 2018. Positive values (blues) indicate increased elevation, and negative values (reds) indicate decreased elevation between the two years. Imagery courtesy of the Geological Survey of Canada.

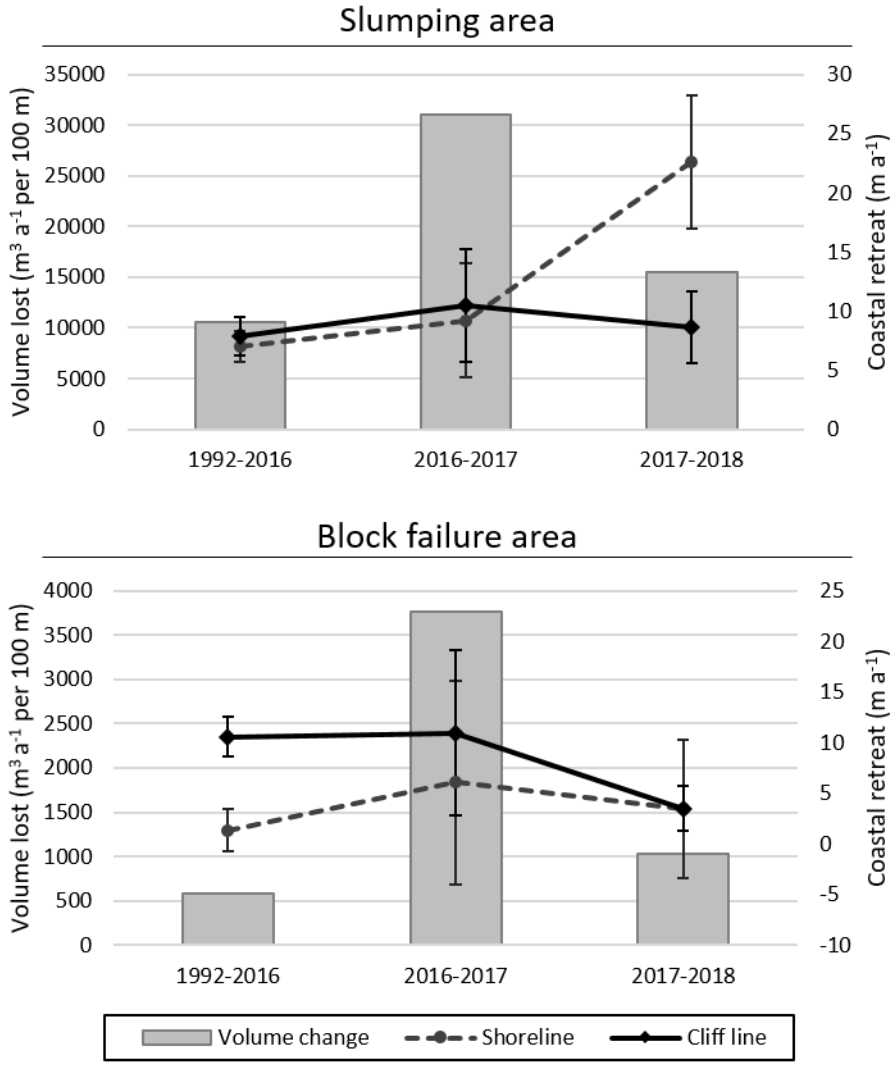

Fig. 8. Mean annual volume change per 100 m of shoreline between consecutive Digital Surface Models from 1992, 2016, 2017, and 2018. Mean annual rates of cliff and shoreline retreat are also shown, with error bars of 1 standard deviation.

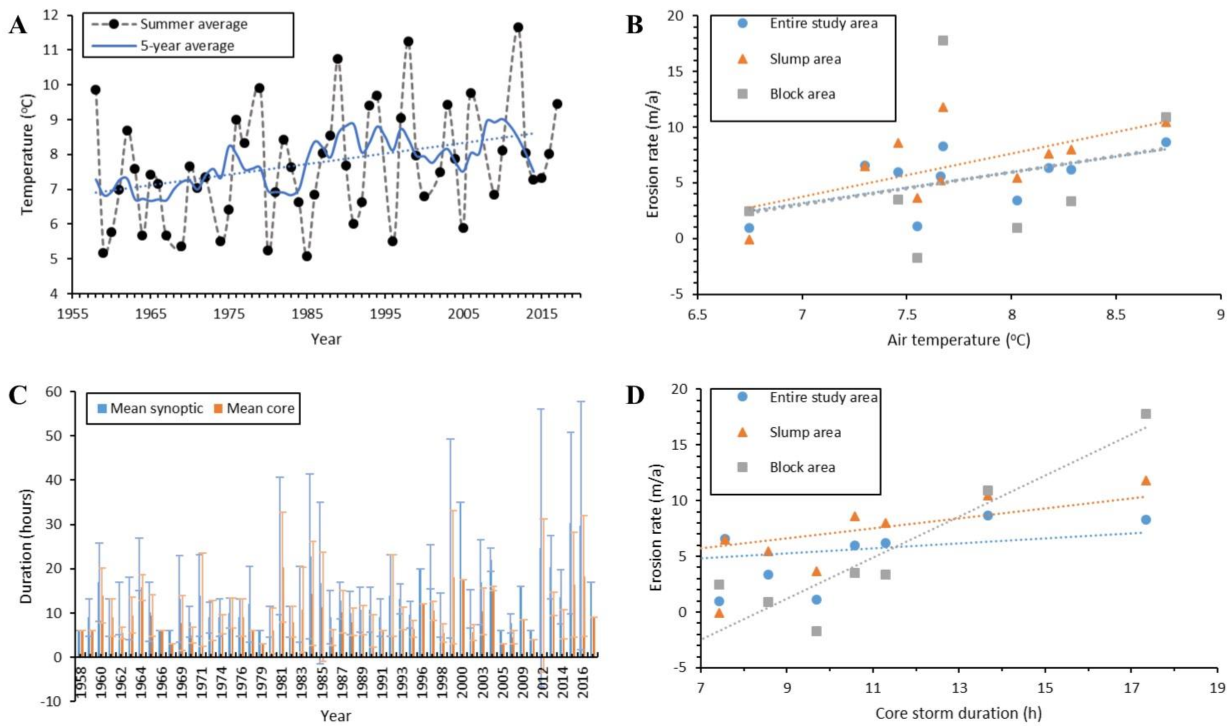

Fig. 9. (A) Mean July to September air temperature measured at Tuktoyaktuk, N.W.T. Note the overall increasing trend (0.03 ºC a^{-1}, r^2=0.56). (B) Mean summer air temperature compared to mean cliff retreat across the entire study area (2.78 m a^{-1} ºC^{-1}; r^2=0.34), the area dominated by slumping (3.90 m a^{-1} ºC^{-1}; r^2=0.41), and the area dominated by block failure (2.90 m a^{-1} ºC^{-1}; r^2 = 0.08). (C) Mean annual synoptic and core storm duration. Error bars represent one standard deviation from the mean. There is a weak positive trend in synoptic duration (10 minutes a^{-1}, r^2= 0.19). There is no trend in core storm duration. (D) Mean core storm duration compared to mean cliff retreat across the entire study area (0.22 m a^{-1} h^{-1}; r^2= 0.13), the area dominated by slumping (0.45 m a^{-1} h^{-1}; r^2= 0.34), and the area dominated by block failure (1.84 m a^{-1} h^{-1}; r^2= 0.84).

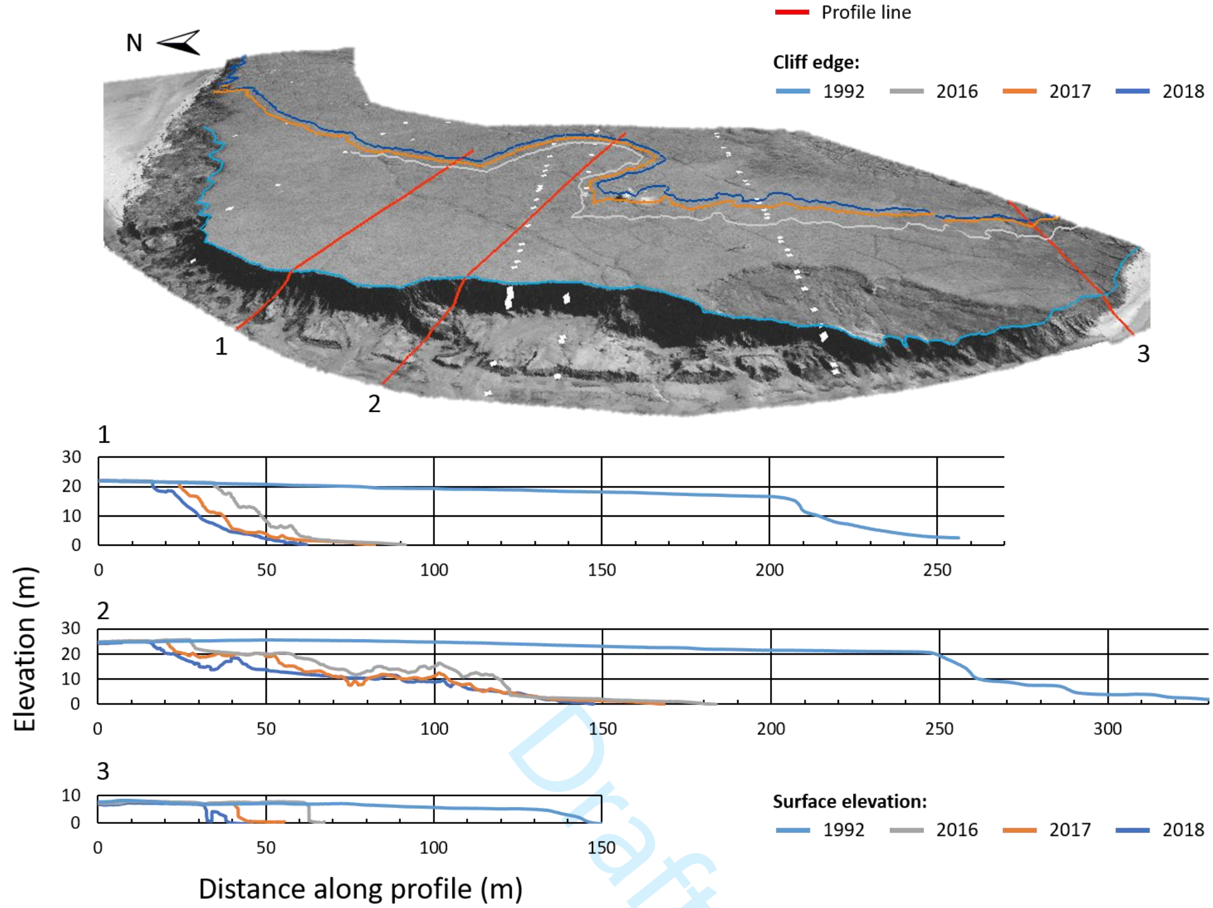

Fig. 10. Elevation profiles through (1) slumping coastal cliffs, (2) active retrogressive thaw slump, and (3) block failure cliff sections based on photogrammetric digital surface models of Pullen Island in 1992, 2016, 2017, and 2018. Profile locations are shown on oblique view of 1992 imagery (courtesy of Geological Survey of Canada).

Region	Mean (m a^{-1})	Standard deviation (m a^{-1})
Outer Mackenzie Delta	1.77	1.82
East Richards Island	0.4	0.62
Outer Mackenzie Delta Islands	1.51	2.79
West Richards Island	0.46	0.79
Tuktoyaktuk Peninsula	0.75	1.28

Year	Pixel size (m)	RMS positional error (m)
1947	1.35	6.09
1950	1.29	5.14
1967	1.29	4.09
1974	1.88	4.55
1985	4.67	7.87
1992	0.25	2.45
2004	0.5	1.76
2016	0.025	0.48
2017	0.025	0.29
2018	0.025	-

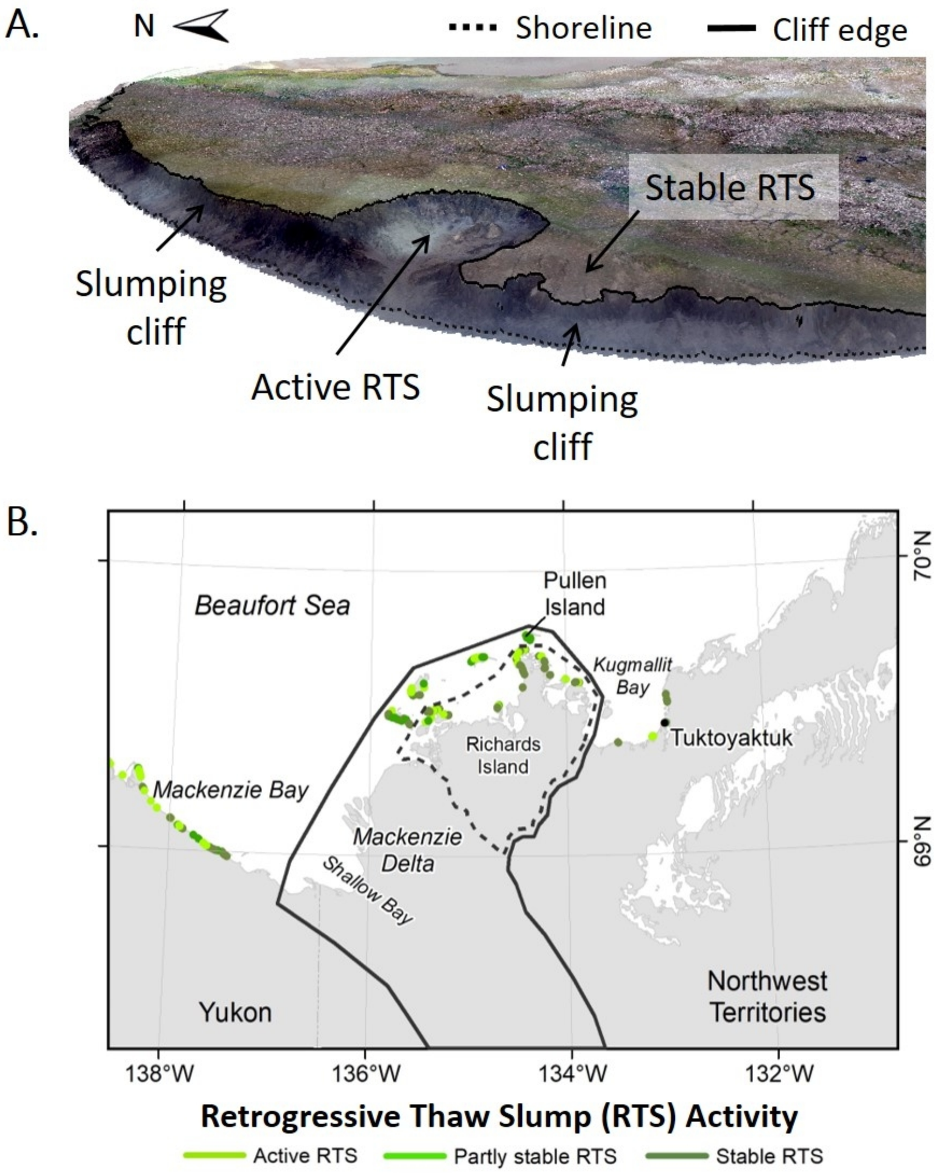

Fig. 1. (A) Oblique view of an active retrogressive thaw slump (RTS), stable RTS, and slumping coastal cliffs on Pullen Island, Northwest Territories (imagery courtesy of the Geological Survey of Canada, 2018). (B) Active, partially stable, and stable RTS occurrences in the Mackenzie Delta region of the Canadian Beaufort Sea coast (Couture, et al., 2015).

152x188mm (150 x 150 DPI)

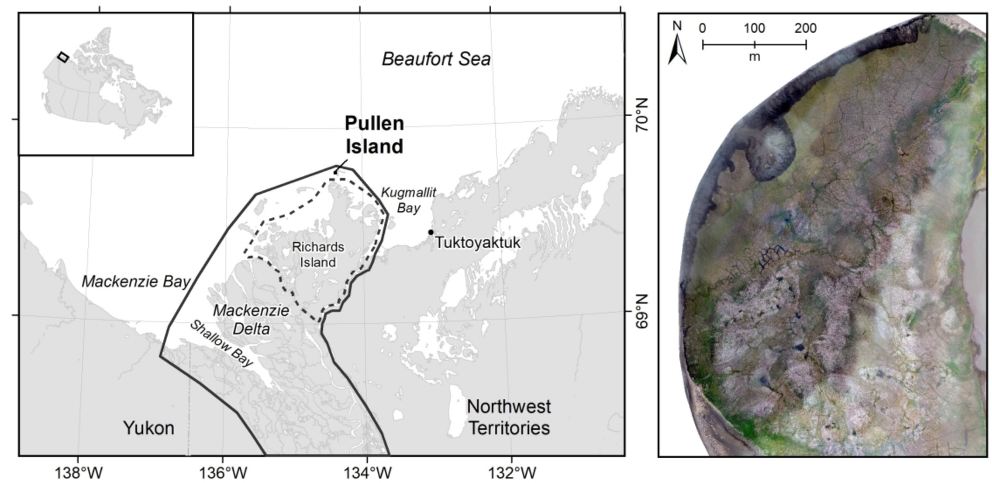

Fig. 2. Location of Pullen Island on the Mackenzie Delta, N.W.T. Aerial imagery courtesy of the Geological Survey of Canada (2018) and base imagery from Statistics Canada (2016a; 2016b).

822x404mm (96 x 96 DPI)

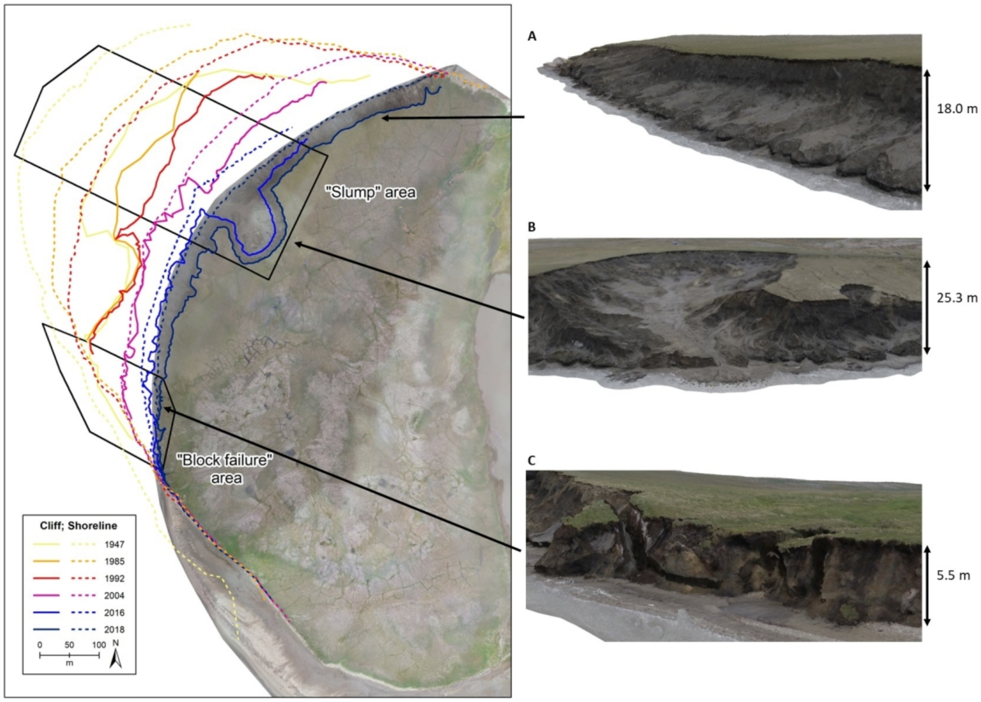

Fig. 3. Location of cliff and shorelines on Pullen Island, N.W.T., 1947-2018. Lines from 1950, 1967, 1974, 2013, 2014, 2015, 2017 excluded for simplicity. Outlined are areas designated as dominated by slump or by block failure for erosion rate comparison. Oblique images show sections of (A) slumping coastal cliffs, (B) retrogressive thaw slumping, and (C) block failure, as seen in the 2018 3D model. Imagery courtesy of the Geological Survey of Canada (2018)

289x215mm (150 x 150 DPI)

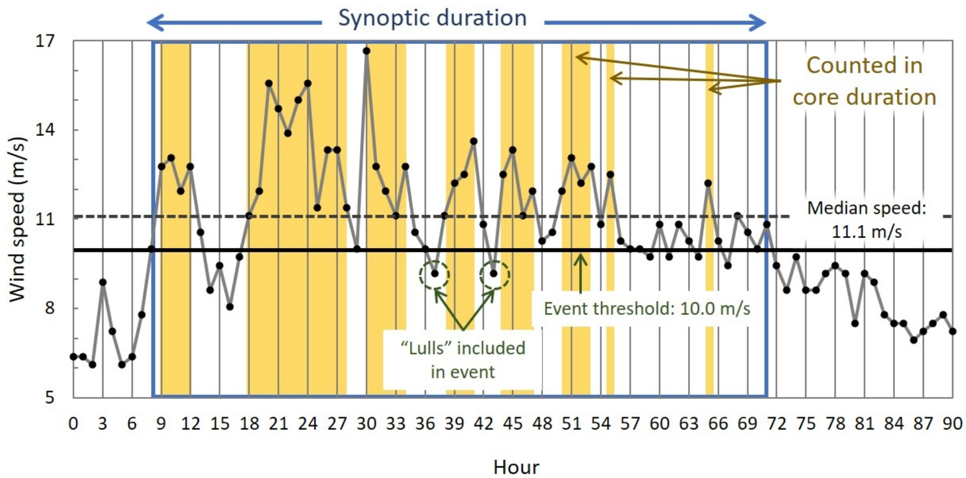

Fig. 4. An example storm event (July 18-21, 2016; Environment and Climate Change Canada, 2016) to illustrate threshold wind speeds in definition of synoptic and core storm duration, per Atkinson (2005). The entire storm event is contained within the blue box, the length being equal to the synoptic duration. Periods during which the wind speed is equal to or greater than the median speed for the event, highlighted in yellow, are counted into the core duration.

213x104mm (150 x 150 DPI)

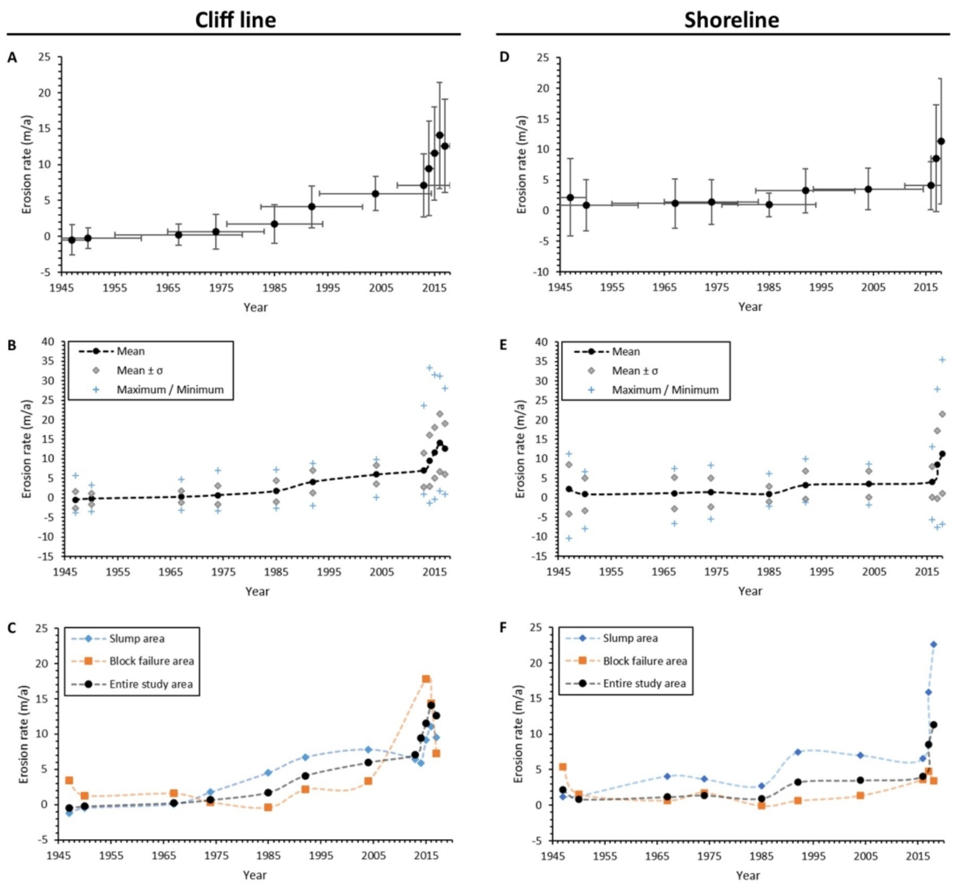

Fig. 5. Mean annual erosion rates on Pullen Island, N.W.T., 1947-2018. (A) Mean cliff line erosion rate of the entire study area. Horizontal error bars are proportional to the number of years over which the measurements are averaged, and vertical error bars are proportional to the positional error of the source data. (B) Mean, maximum, minimum, and standard deviation of the annual cliff erosion rates for the entire study area. (C) Mean rate of cliff retreat in the slumping and block failure areas. (D) Mean shoreline erosion rate of the entire study area. Horizontal error bars are proportional to the number of years over which the measurements are averaged, and vertical error bars are proportional to the positional error of the source data. (E) Mean, maximum, minimum, and standard deviation of the annual shoreline erosion rates for the entire study area. (F) Mean rate of shoreline retreat in the slumping and block failure areas.

320x297mm (150 x 150 DPI)

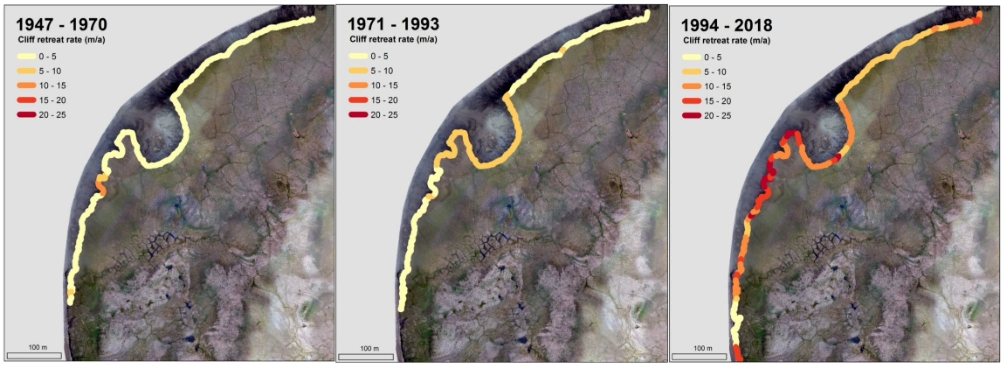

Fig. 6. Mean rate of annual cliff retreat through time. Focusing on the northwest area of Pullen Island, mean rates for each time period (1947-1970, 1971-1993, 1994-2018) are displayed on an equal interval scale of 5 m a^{-1}. Imagery courtesy of the Geological Survey of Canada (2018)

540x195mm (150 x 150 DPI)

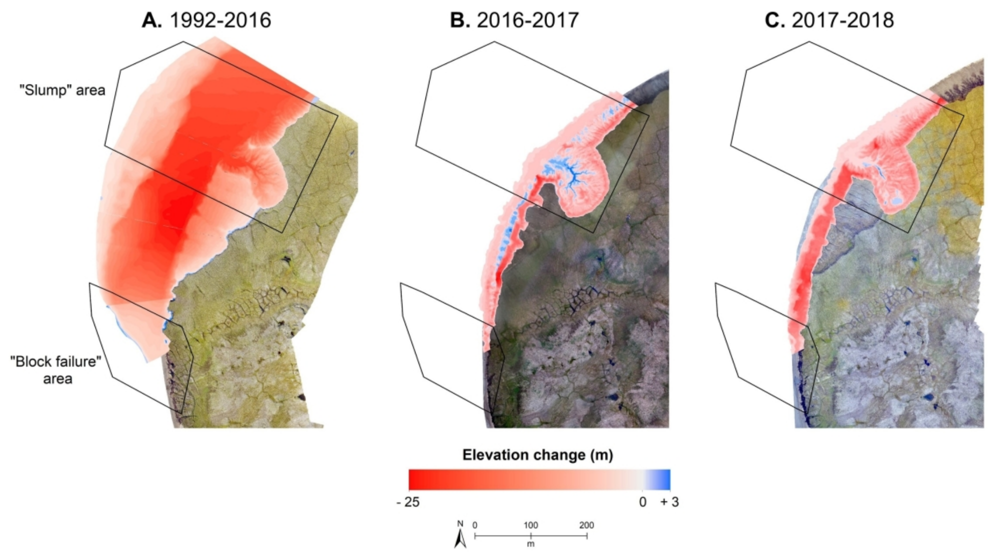

Fig. 7. Elevation difference between Digital Surface Models over (A) 1992-2016, shown over imagery from 2016; (B) 2016-2017, shown over imagery from 2017; and (C) 2017-2018, shown over imagery from 2018. Positive values (blues) indicate increased elevation, and negative values (reds) indicate decreased elevation between the two years. Imagery courtesy of the Geological Survey of Canada.

719x407mm (96 x 96 DPI)

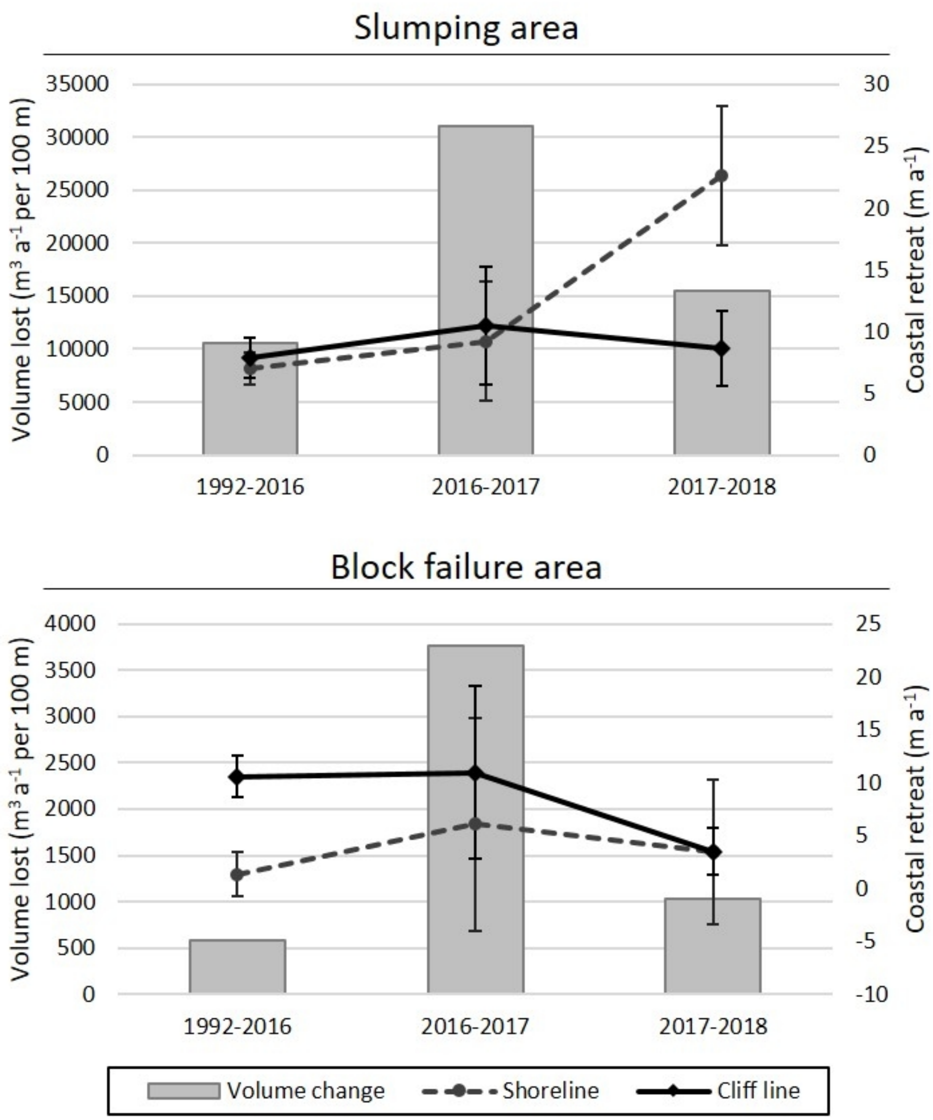

Fig. 8. Mean annual volume change per 100 m of shoreline between consecutive Digital Surface Models from 1992, 2016, 2017, and 2018. Mean annual rates of cliff and shoreline retreat are also shown, with error bars of 1 standard deviation.

126x144mm (150 x 150 DPI)

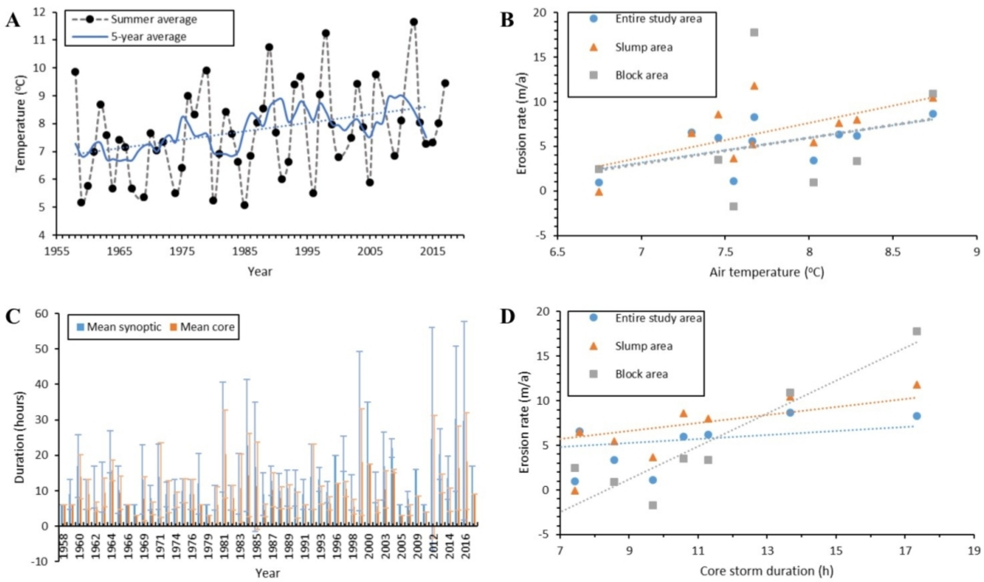

Fig. 9. (A) Mean July to September air temperature measured at Tuktoyaktuk, N.W.T. Note the overall increasing trend (0.03 °C a^{-1}, r^2=0.56). (B) Mean summer air temperature compared to mean cliff retreat across the entire study area (2.78 m a^{-1} °C^{-1}; r^2=0.34), the area dominated by slumping (3.90 m a^{-1} °C^{-1}; r^2=0.41), and the area dominated by block failure (2.90 m a^{-1} °C^{-1}; r^2 = 0.08). (C) Mean annual synoptic and core storm duration. Error bars represent one standard deviation from the mean. There is a weak positive trend in synoptic duration (10 minutes a^{-1}; r^2= 0.19). There is no trend in core storm duration. (D) Mean core storm duration compared to mean cliff retreat across the entire study area (0.22 m a^{-1} h^{-1}; r^2= 0.13), the area dominated by slumping (0.45 m a^{-1} h^{-1}; r^2= 0.34), and the area dominated by block failure (1.84 m a^{-1} h^{-1}; r^2= 0.84).

254x152mm (150 x 150 DPI)

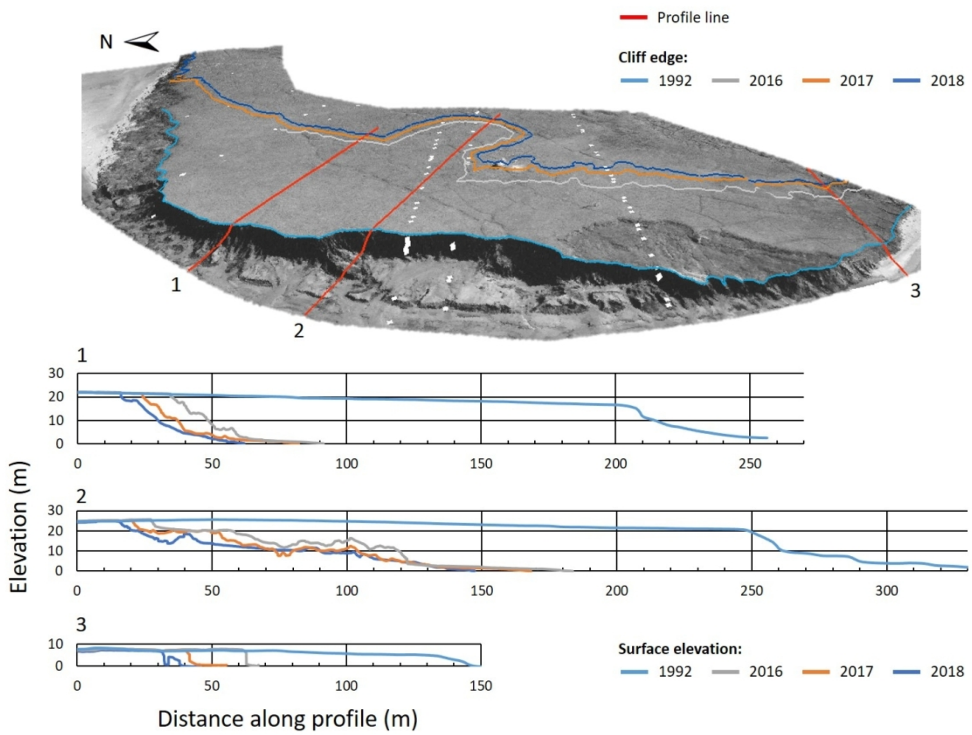

Fig. 10. Elevation profiles through (1) slumping coastal cliffs, (2) active retrogressive thaw slump, and (3) block failure cliff sections based on photogrammetric digital surface models of Pullen Island in 1992, 2016, 2017, and 2018. Profile locations are shown on oblique view of 1992 imagery (courtesy of Geological Survey of Canada).

254x191mm (150 x 150 DPI)